AI and Machine Learning in Healthcare and Biomedical Engineering

AG EDITOR

AI and Machine Learning in Healthcare and Biomedical Engineering

Vugar Abdullayev (Ed.)

Alex Khang (Ed)

AG EDITOR

Copyright Page

© 2025. The authors. This is an open access book, distributed under the terms of a Creative Commons Attribution 4.0 license (https://creativecommons.org/licenses/by/4.0) that allows use, distribution, and reproduction in any medium provided that the original work is properly cited.

This AG Editor imprint is published by AG Editor.

The registered company is **AG Editor SAS, Montevideo, Uruguay.**

For more information, see AG Editor's Open Access Policy: https://www.ageditor.org/editorial-policies.php

ISBN (eBook): 978-9915-704-01-2

ISBN (Softcover): 978-9915-704-02-9

This title is available in both print (softcover) and digital (open access PDF) formats.

DOI: 10.62486/978-9915-704-01-2

Publisher: Javier González Argote
Chief Executive Officer: editorial@ageditor.org
Editorial Director: Emanuel Maldonado
Editorial Coordinators: William Castillo González; Karina Maldonado
Production Manager: Adrian Vitón Castillo

Legal Deposit: National Library of Uruguay — Law No. 13.835/1970 and Decree No. 694/1971

ISBN Record: National ISBN Agency (Uruguay) — Filing No. 58241

Cataloging Data

Cataloging-in-Publication Data (CIP):
AG Editor
AI and Machine Learning in Healthcare and Biomedical Engineering / edited by Vugar Abdullayev and Alex Khang. – Montevideo: AG Editor, 2025.

ISBN (eBook): 978-9915-704-01-2

ISBN (Softcover): 978-9915-704-02-9

THEMA classification codes:
UYQE – Expert systems / knowledge-based systems

Editorial Notice and Acknowledgments

The publication of this book is part of AG Editor's mission to promote open, ethical, and rigorous scientific communication across all areas of knowledge.

All books published by AG Editor undergo a double-blind peer-review process and a technical evaluation in accordance with the publisher's editorial policies, aligned with COPE and ICMJE standards.

AG Editor acknowledges the valuable collaboration of authors, reviewers, designers, and production teams who made this publication possible.

Preface

Over the past decade, artificial intelligence (AI) and machine learning (ML) have moved from being promising research topics to becoming indispensable tools across the healthcare ecosystem. From diagnostic imaging and computer-aided decision support to connected medical devices and implantable systems, AI is progressively reshaping how we sense, interpret, and act on biomedical information. Yet, translating algorithms into clinically meaningful, robust, and energy-efficient solutions remains a complex, multidisciplinary challenge—one that sits at the intersection of medicine, electrical and biomedical engineering, computer science, and applied mathematics.

This edited volume, AI and Machine Learning in Healthcare and Biomedical Engineering, was conceived as a contribution to that intersection. The chapters compiled here explore how AI and ML can be embedded across the full pipeline of modern healthcare technologies: from the enhancement and fusion of medical images, through intelligent classification and decision-making, down to the optimization of the analog front-ends and low-noise amplifiers that acquire and transmit physiological signals.

Several chapters focus on medical imaging for oncology, particularly brain and lung tumors. One contribution presents a structured preprocessing and enhancement pipeline for MRI brain tumor images using filtering, adaptive histogram equalization, and wavelet-based techniques to improve signal-to-noise ratio and structural similarity, thereby enabling more accurate segmentation and classification in downstream models. Another chapter addresses lung cancer diagnosis, proposing deep convolutional neural network architectures for the classification of lung nodules in CT images into benign and malignant categories, demonstrating high diagnostic accuracy on widely used clinical datasets.

Beyond single-modality processing, the book includes work on multimodal fusion techniques that combine MRI and PET data using hybrid transform and dimensionality reduction frameworks together with fine-tuned deep models. These contributions show that intelligently fused images can achieve strong image quality metrics and excellent classification performance, highlighting how multimodal integration strengthens clinical decision-making for tumor characterization.

A second thematic axis of the book is AI-enabled modeling and classification frameworks for brain tumor MRI. Several chapters analyze how hybrid pipelines that couple CNN-based deep feature extractors with classical classifiers such as support vector machines and random forests can outperform stand-alone deep networks, especially under limited data conditions—a frequent reality in medical imaging. These hybrid systems reach high accuracy and F1-scores, illustrating the value of combining deep representations with interpretable, well-understood classical models. Complementary work delves into feature extraction and selection for brain tumor MRI, integrating textural, frequency-based, and deep features with dimensionality reduction and evolutionary algorithms to construct compact, highly discriminative feature sets.

The third axis of the volume shifts focus from algorithms to hardware and biomedical front-ends, where AI supports the design of circuits that form the physical interface

with the human body. One chapter reviews how machine learning can assist the optimization of low-noise amplifiers (LNAs) for medical IoT devices, addressing multi-objective trade-offs among noise figure, gain, bandwidth, power consumption, and linearity. It shows that ML-guided optimization can achieve lower noise figures, improved gain-versus-power trade-offs, and faster convergence in the design space, thereby shortening development cycles and enhancing performance in wearable and remote-monitoring applications. Another chapter presents a current-reuse narrowband LNA for the MICS band (402–405 MHz), analyzing its parameters and noise behavior through an analytical framework and demonstrating gain and noise performance compatible with state-of-the-art implantable medical devices.

Taken together, these contributions provide a coherent panorama of how AI and ML can be integrated across the stack: at the signal and image level, enhancing, denoising, and fusing data to expose diagnostically relevant structures; at the model level, combining deep and classical approaches to achieve robust, explainable classification of tumors and other pathologies from MRI and CT data; and at the hardware and systems level, leveraging machine learning to systematically explore complex analog and RF design spaces for medical IoT and implantable communication.

Our intended audience includes graduate students, researchers, and practitioners in biomedical engineering, electrical and electronics engineering, computer science, and related health technologies, as well as clinicians interested in understanding the capabilities and limitations of AI-driven tools. Each chapter is self-contained and can be read independently; however, readers will gain the greatest benefit by considering the cross-cutting themes that emerge across sections: the importance of high-quality data and preprocessing, the role of feature engineering even in the deep-learning era, the need for careful evaluation metrics, and the practical constraints of real-world medical systems, including latency, power, interpretability, and regulatory considerations.

We hope that this book serves not only as a reference to current methods but also as an invitation to further dialogue and collaboration between engineers, data scientists, and healthcare professionals. The future of AI in healthcare will be defined not by algorithms alone, but by how effectively we align those algorithms with clinical workflows, patient needs, and ethical frameworks. We are grateful to all the authors for their rigor and commitment, and to the readers who will carry these ideas into new applications and innovations.

Vugar Abdullayev
Alex Khang
Editors

Abstract

AI and Machine Learning in Healthcare and Biomedical Engineering presents a collection of recent research at the intersection of artificial intelligence, medical imaging, and biomedical hardware design. The volume focuses on two tightly coupled domains: AI-driven analysis of oncological imaging (with an emphasis on brain and lung tumors) and machine-learning-assisted optimization of low-noise front-ends for medical Internet of Things (IoT) devices and implantable systems.

On the imaging side, several chapters propose advanced pipelines for preprocessing and enhancing MRI and CT data, including filtering, contrast enhancement, and transform-based techniques, as well as multimodal MRI–PET fusion. These methods aim to improve image quality and tumor boundary visibility, facilitating more reliable segmentation and diagnosis. Building on these foundations, the book explores deep and hybrid learning models—convolutional neural networks combined with classical classifiers—as well as feature extraction and selection strategies that integrate textural, frequency-based, and deep representations. Experiments on benchmark datasets for brain and lung tumors show that these approaches can achieve high accuracy and robust performance, underscoring the diagnostic potential of AI-based methods.

At the hardware level, the book examines how machine learning can guide the design of low-noise amplifiers for medical IoT and implantable communication in medically allocated frequency bands. The chapters demonstrate that data-driven optimization can reduce noise figures, improve gain-versus-power trade-offs, and accelerate convergence in multi-objective design spaces, yielding LNAs with performance suitable for low-power wearable and implantable devices.

By bringing together methods for image enhancement, multimodal fusion, feature engineering, classification, and hardware optimization, this edited volume offers an integrated view of how AI and machine learning can be embedded throughout the sensing, processing, and communication chain in modern healthcare systems. It is intended for researchers, graduate students, and practitioners in biomedical engineering, medical imaging, electronics, and health informatics who seek both methodological insight and application-oriented case studies.

Keywords: Artificial intelligence, Machine learning, Medical imaging, Brain tumors, Lung cancer, Biomedical engineering, Medical Internet of Things (IoT), Implantable medical devices

Index

Chapter 01

AI and Machine Learning in Healthcare and Biomedical Engineering
ISBN: 978-9915-704-01-2
DOI: 10.62486/978-9915-704-01-2.ch01
Pages: 1-9

©2025 The authors. This is an open access article distributed under the terms of the Creative Commons Attribution (CC BY) 4.0 License.

Classification of Lung Nodules on CT Images by Employing Machine and Deep Learning Techniques

Jarupula Somlal[1] ✉, N Narender Reddy[2] ✉, Sk Hasane Ahammad[3] ✉, Ebrahim E. Elsayed[4] ✉, Davron Juraev[5,6,7,8] ✉, Nazila Ragimova[9], Vugar Abdullayev[9] ✉

[1]Department of EEE, Koneru Lakshmaiah Education Foundation. Guntur, India-522302.
[2]Faculty of Degree Engineering, Military College of Electronics and Mechanical Engineering. Secunderabad, Telangana.
[3]Department of ECE, Koneru Lakshmaiah Education Foundation. Guntur, India-522302.
[4]Department of ECE, Faculty of Engineering, Mansoura University. Mansoura, Egypt.
[5]Scientific Research Center, Baku Engineering University. Baku AZ0102, Azerbaijan.
[6]Scientific Laboratory of Dynamical Systems and Their Applications, Institute of Mathematics Uzbekistan Academy of Sciences. Tashkent 100174, Uzbekistan,
[7]Postdoctoral Department, Turon University. Karshi 180100, Uzbekistan.
[8]Scientific Department, University of Economics and Pedagogy. Karshi 180100, Uzbekistan.
[9]Azerbaijan State Oil and Industry University. Azerbaijan.

Corresponding author: Ebrahim E. Elsayed ✉, Vugar Abdullayev ✉

ABSTRACT

In the current scenario, cases of lung cancer are rapidly increasing. As per the statistical analysis of 2020, due to this effect, it almost accounts for 10 million approximate deaths. Mostly, lung cancer is diagnosed or identified at early stages based on the doctor's expertise. In the current research, computed tomography (CT) is the helping hand for doctors to pinpoint or detect cancerous lungs at the beginning stage itself. Moreover, Deep learning and machine learning techniques are widely applied for various diagnoses under the medical imaging process due to their powerful outcomes. This study deals with the architecture of deep neural for classifying the lung nodule. The networks are integrated within the classification challenge of CT images for the type of lung nodule (benign & malignant). Further, evaluation is done through the database of LIDC-IDRI. The study Convolutional Neural Network (CNN) approach for tumour classification. Moreover, the CNN precision has reached an efficiency of 95 %, corresponding with conventional systems. As a result, Machine learning methods and deep learning techniques formed a base for image processing applications for estimating the level of cancer in patients affected. Furthermore, the proposed system is supported in detecting the effect at early stages.

Keywords: Deep Learning; Machine Learning; CT; Lung Nodule; Detection; Classification; Diagnosis.

INTRODUCTION

Worldwide, lung cancer is the frequent dead causing effect, occurring in both genders.[1] Reports in 2021 say that newly entered lung cancer cases are about 198 200 within the mortality rate exceeded the threshold value. Due to this incident, it is evident to examine the lung nodule for every stage of the affected region. With this detection under early diagnosis, the rate of survival within the 5-year can be enhanced by the value of 60 %.[2] In this light, the most efficient methodology that has come into the picture for proving its ability in diagnosing the defect is through Computed tomography (CT) scan, which is the three-dimensional (3D) images,

which outcomes towards better resolution in tumor pathology and of nodules.[3,4] Furthermore, the CT image can support several diagnostics extensively utilized in clinical applications.[5]

Moreover, the classification under the computer-aided diagnosis (CAD) process for lung cancer is categorized into the system of detecting the overall system involved under the analysis. Most recently, the neural network process, also termed to be one of the categories of deep learning, initiated knocking conventional AI technology almost for every challenge that has undertaken few featuring aspects such as recognizing speech, generating natural, characterizing images, readable sentences.[6,7] Therefore, the overall assessment under the technology of deep learning doesn't enable the critical challenge acceleration but rather enhances the computer behaviour in classifying or detecting the effect through CT images.[4] Thus, the focus is more on categorizing the type of cancer considered is benign and malignant. It is observed that most research under this area is employed through the techniques like deep neural network (DNN), convolution neural network (CNN), and stacked autoencoder (SAE). With this effect, the proportion change can reduce reframing the data that has been processed for feature extraction and classification. The instant in which cells migrate with remaining tissues there occurs metastasis. As soon as probable, at early stages, cancer can be identified to avoid the greater spread in affecting the health of the person.[8] Lung cancer diagnostics is highly severe symptoms that only can be observed at the last stage of effect. Therefore, it is merely intolerable to protect the life of a person. To examine the lungs for capturing the techniques associated with the CT, Magnetic resonance imaging (MRI), X-ray, and Positron Emission Tomography (PET). The imaging technique involved for the CT is mainly utilized for the structure case integrated into the overlapped outline.[9] For the CT images of lung cancer, the accuracy is reached in the photograph resolution through the superior knowledge of the methodology. To recognize lung cancer at the beginning level, image processing techniques and deep learning methods are employed. Further, the detection of tumours, then the shape, location, and dimension can be detected in the earlier challenge. By enhancing the computation time with adequate technology, the patient treatment will be efficiently operated. The following represents the loss function mathematically,

$$c(w,b) = \frac{1}{2n}\sum_x ||y(x) - a||^2 + \frac{1}{2n}\lambda \sum_w w^2 \qquad (1)$$

The value of C gives the expression for cost function, with weighing factor of w and bias parameter b with estimated cost value for the training count of the instance dataset within the pixel value of image to attain the value of output. Functionally, the activation value is associated to the non-linear modelling of the neural network, the expression will be as follows:

$$y = \begin{cases} x \; if \; x \geq 0 \\ 0 \; if \; x < 0 \end{cases} \qquad (2)$$

The study will undergo the initial steps that include the stages of preprocessing, postprocessing, and classification methods that account for the tumor classification for various categories such as Malignant and Benign. The tumor non-cancerous tend to be benign that not allow the propagation to the remaining parts. Besides, lung cancer diagnostics is highly severe symptoms that only can be observed at the last stage of effect. Therefore, it is merely intolerable to protect the life of a person. To examine the lungs for capturing the techniques associated with the CT, Magnetic resonance imaging (MRI), X-ray, and Positron Emission Tomography (PET).[10] The

imaging technique involved for the CT is providently utilized for the structure case integrated into the overlapped outline. For the CT images of lung cancer, the accuracy is reached in the photograph resolution through the superior knowledge of the methodology. Further, inconsistent cells can be separated together in the absence of monitoring into which the tissues can be invaded subsequently within the tissues surrounded.[11] Thus, foreseeing the various procedures for lung cancer diagnosis can be objected to the study. The overall structure involved in the CAD system depicted in figure 1.1 is represented with support to the process's steps.

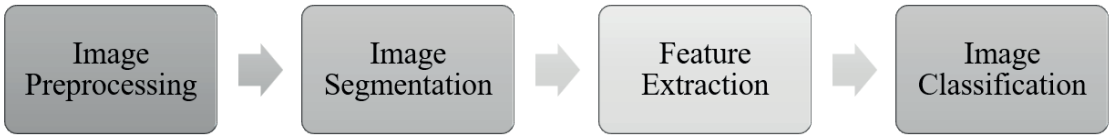

Figure 1.1. Elementary Phases in CAD System

Typically, the Lung CADs are classified based on the circumstances: background-oriented segment nodules, individual segments extracted the features associated under the nodule and features utilization for characterizing the classifier into the nodule form of benign or possibly malignant. Conventional segmentation techniques for lung nodules include identification, detection, and region of interest (ROI) segmentation for nodule incorporation. Further, the procedures can be portioned based on the optimization. The region developed morphologic situations and statistical learning methods. Nevertheless, nodule segmentation challenge can be affected through connections among nodules along with other lung formations. During the early stages, lung cancer detection utilizing CT scans support many individual lives. However, evaluating the majority of scans remains unsatiated for radiologists. Therefore, a Deep Convolutional Neural Network (DCNN) combined with several techniques under preprocessing stage for building the automated Lung nodules prediction precision rate coupled with Malignancy applying CT scans. Also, the methodology attains for enhanced performance of object detection in biological images, within the account of techniques related to the state-of-the-art application in medical imaging and object detection.

METHOD

The image pixel consistency can be achieved through the techniques profuse within the observation of the similitude group. Within the features of various kurtosis of the methodology in extracting the feature to analyze the deviation in the region of the segmentation process. The structural framework for the deep learning process is depicted in figure 1.2.[5] The CT image can undergo support for several diagnostics extensively utilized in clinical applications through computer processing. Moreover, the classification under the computer-aided diagnosis (CAD) process for the effect of lung cancer is categorized into the system of detecting the overall system involved under the analysis.[12] The tumor of non-cancerous tends to be benign that not allow the propagation to remaining parts. Besides, lung cancer diagnostics is highly severe symptoms that only can be observed at the last stage of effect.[13]

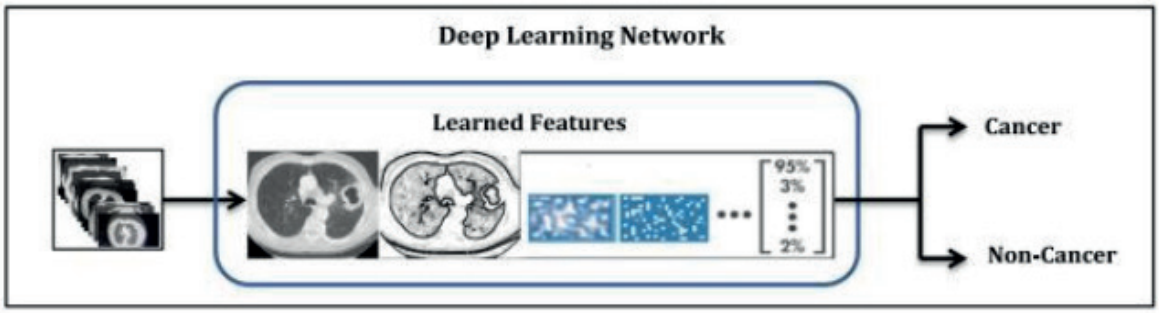

Figure 1.2. Structural framework of Deep learning method

To examine the lungs for capturing the techniques associated with the CT, Magnetic resonance imaging (MRI), X-ray, and Positron Emission Tomography (PET). The imaging technique involved for the CT is mainly utilized for the structure case integrated into the overlapped outline.[13] For the CT images of lung cancer, the accuracy is reached in the photograph resolution through the superior knowledge of the methodology. Furthermore, to recognize lung cancer at the beginning level, techniques of image processing and deep learning methods are employed.[14]

For the CNN, the dimension of the layers fed as input is about m x n x r, in which r denotes the channel count. With the dimension of n x n x q, the kernel is associated within the field of filtering the region under the range of $n < m$, $q \leq r$, and alters with every kernel associated under CNN with mapping a feature. In the provision of mapping the elements, the subsampled image can undergo the mean range of about 3 to 6 under the non-linearity of the subsampling layer. Primarily, the regions of lung cancer can be extracted through the CT images within each phase for further segmentation of the tumor for additional architecture training of CNN. Thus, testing the pictures of each patient.

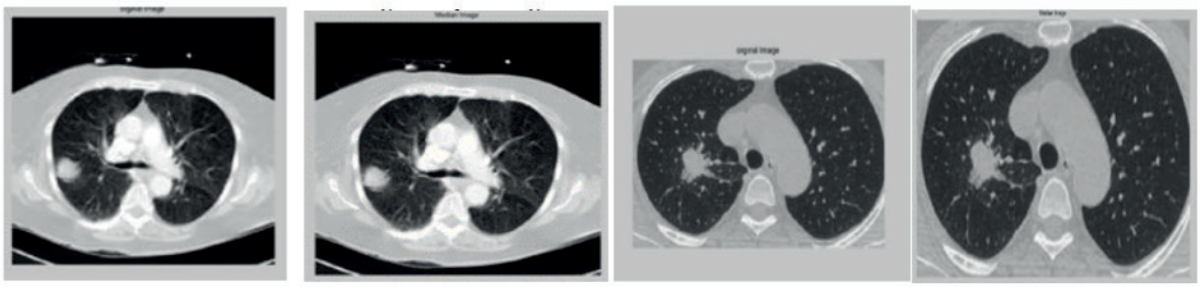

Figure 1.3. Input Image and Median Filtered

In the database's Cancer Imaging Archive (TCIA), LIDC-IDRI encompasses 1029 clinical chest CT scans, including lung nodules taken from 8 organizations integrated within the file format of XML that features the nodule's location.

RESULTS AND DISCUSSION

Implementing the neural network-based segmentation, the classifications of lung nodules will be effectively utilized for the early-stage detection. The entire process is simulated through MATLAB software. In addition, the plant or process has been trained by various sample datasets

to model and understand the performance of methodology. For instance, the sample image as the input introduced within the models at each stage for the province of cancerous cells in the tissues allocated with various dimensions to spot the same view.[15]

To analyse the neural network, the ROC curve has been implemented. The end-to-end process is involved in the learning process for detecting lung cancer through CNN since it incorporates weights initialization, gradient moment, and Learning rate, in addition to hidden neurons. Whatever modifications attain with the neural network of hidden layers, matrix reached zero for the valued matrix articulated within the parameters built with. Key parameters that are utilized for the model to be trained in the CNN is listed below.

Thus, the image application follows the preprocessing stage, feature extraction, recognizing or classifying the spot of cancer, besides outcomes the user benefit from the appropriate diagnosis. Once the simulation outputs with the indication of the screened display as shown in the figure below, it is confirmed that Malignancy exists, laterally with the input image fed.

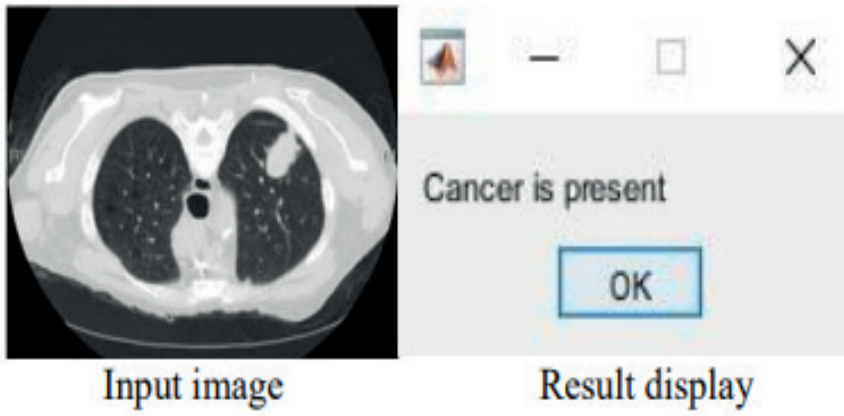

Figure 1.4. Output for Cancerous Image

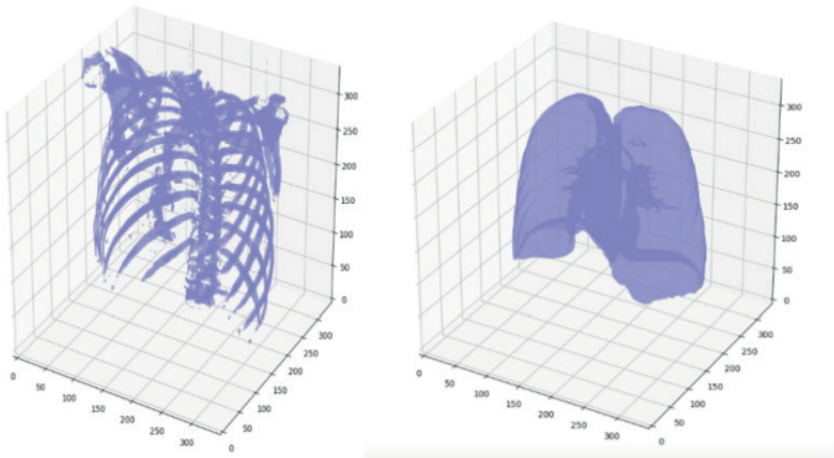

Figure 1.5. 3D mapped CT scan and Segmented lung area

Table 1.1. Parameters fed for the model training of Deep Neural Network

Parameter	Estimate
Weight	0,000019
Learning rate	0,00001
Bias	0,9
Gradient moment	0,85
Hidden moment	249
Epoch	99

In order to increase the comparability, the experiments in the paper are done in the same data set, as well as the comparison of the same parameters. By contrast, the experimental data and the results of the CNN architecture have made some progress. The process can be extended with the same proposed system under the larger dataset to identify or analyze the cancer nature based on the dimension and shape or region.[6] Furthermore, the result shows that the proposed system's accuracy is enhanced by exploiting 3D CNN and enlightening deep networks integrated by the hidden neurons.[2,12]

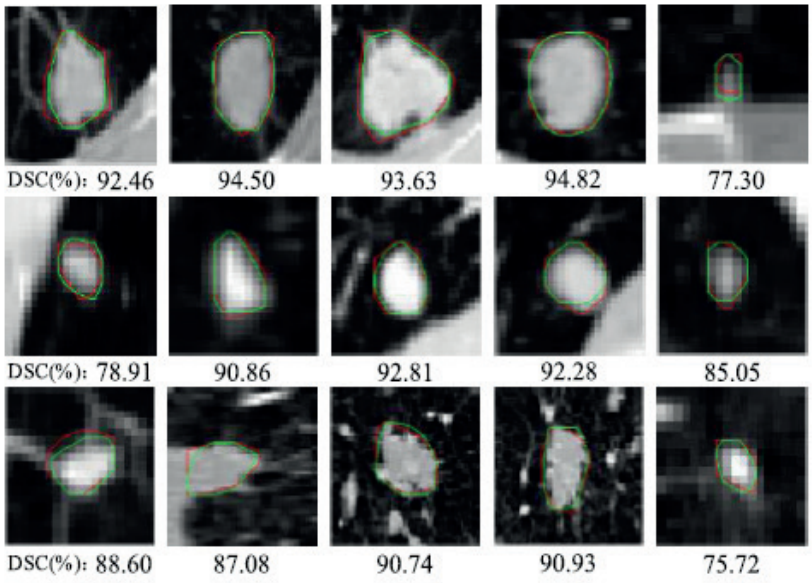

Figure 1.6. Randomly chosen lung nodules from the testing dataset with the segmentation outcomes

CONCLUSION

The study focuses on the machine and deep learning techniques for the classification of Lung Nodules through the input of CT Images, thus evaluating the extensive outcome through the integration of neural networks. The networks are integrated within the classification challenge of CT images for the type of lung nodule (benign & malignant). Moreover, classification of the pulmonary nodules within the category of benign and malignant underwent the comparison through the database of LIDC-IDRI. Further, experimental results recommend that précised performance is achieved through CNN based methodology instead of DNN and SAE. Furthermore, the methods proposed can identify the cancerous cells within the precision rate of 95 %. As a result, Machine learning methods, in addition to deep learning techniques, formed as a base for

the image processing applications

REFERENCES

1. GLOBOCAN. Fact sheets: cancer statistics. http://globocan.iarc.fr/Pages/fact_sheets_cancer.aspx

2. LiveMint. India recorded about 3.9 million cancer cases in 2016. https://www.livemint.com/Politics/3eXX60XBig4bWZ25Kr1iQO/India-ecordedabout39-million-cancer-cases-in-2016data.html

3. Using deep learning for classification of lung tumors on computed tomography images.

4. Al-Tarawneh MS. Lung cancer detection using image processing techniques. Leonardo Electron J Pract Technol. 2012;20:147–158.

5. LUNA16. Lung tumor analysis challenge 2016. https://luna16.grandchallenge.org/

6. Ahammad SH, Jayaraj R, Shibu S, Sujatha V, Prathima C, Megalan Leo L, et al. Advanced model based machine learning technique for early stage prediction of ankylosing spondylitis under timely analysis with featured textures. Multimed Tools Appl. 2024;83(26):68393–68413.

7. Manikandarajan A, Sasikala S. Detection and segmentation of lymph nodes for lung cancer diagnosis. Proc Natl Conf Syst Des Inf Process. 2013.

8. Chon A, Lu P, Balachandar N. Deep convolutional neural networks for lung cancer detection. Wavelet recurrent neural network for lung cancer classification. Proc 3rd ICST Computer. 2017.

9. El-Baz A, Beache GM, Gimel'farb G, et al. Computer-aided diagnosis systems for lung cancer: challenges and methodologies review article. Int J Biomed Imaging. 2013;2013:942353.

10. Chen H, Wu W, Xia H, Du J, Yang M, Ma B. Classification of pulmonary nodules using neural network ensemble. In: Advances in Neural Networks. Springer; 2011. p. 460–466.

11. Ahammad SK, Rajesh V, Zia Ur Rahman M. Fast and accurate feature extraction-based segmentation framework for spinal cord injury severity classification. IEEE Access. 2019;7:46092–46103.

12. Ahammad SK, Rajesh V, Zia Ur Rahman M, Lay-Ekuakille A. A hybrid CNN-based segmentation and boosting classifier for real time sensor spinal cord injury data. IEEE Sens J. 2020;20(17):10092–10101.

13. Kumar D, Wong A, Clausi DA. Lung nodule classification using deep features in CT images. Proc IEEE Conf Comput Robot Vis. 2015:133–138.

Hinton GE, Osindero S, Teh YW. A fast learning algorithm for deep belief nets. Neural Comput. 2006;18(7):1527–1554.

14. Hua KL, Hsu CH, Hidayati SC, Cheng WH, Chen YJ. Computer-aided classification of lung nodules on computed tomography images via deep learning technique. Onco Targets Ther. 2014;8:2015–2022.

15. Shen W, Zhou M, Yang F, Yang C, Tian J. Multi-scale convolutional neural networks for lung nodule classification. Proc 24th Int Conf Inf Process Med Imaging. 2015:588–599.

CONFLICT OF INTEREST

The authors assert that there are no conflicts of interest related to the research results presented.

FUNDING

This research received no specific grant from any funding agency in the public, commercial, or not-for-profit sectors.

AUTHORSHIP CONTRIBUTION

Conceptualization: Jarupula Somlal, N Narender Reddy, Sk Hasane Ahammad, Ebrahim E. Elsayed, Davron Juraev, Nazila Ragimova, Vugar Abdullayev.

Writing – original draft: Jarupula Somlal, N Narender Reddy, Sk Hasane Ahammad, Ebrahim E. Elsayed, Davron Juraev, Nazila Ragimova, Vugar Abdullayev.

Writing – proofreading and editing: Jarupula Somlal, N Narender Reddy, Sk Hasane Ahammad, Ebrahim E. Elsayed, Davron Juraev, Nazila Ragimova, Vugar Abdullayev.

AI and Machine Learning in Healthcare and Biomedical Engineering
ISBN: 978-9915-704-01-2
DOI: 10.62486/978-9915-704-01-2.ch02
Pages: 10-17

©2025 The authors. This is an open access article distributed under the terms of the Creative Commons Attribution (CC BY) 4.0 License.

Machine Learning-Assisted Optimization of Low Noise Amplifiers for Medical IoT Applications

Saggurthi Spandana[1] ✉, Sk. Hasane Ahammad[1] ✉, Mohammed R. Hayal[2] ✉, Ebrahim E. Elsayed[2] ✉, Nazila Ragimova[3], Bahar Asgarova[3], Vugar Abdullayev[3,4] ✉, Mahbuba Shirinova[3]

[1]Department of ECE, Koneru Lakshmaiah Education Foundation, Green Fields, Andhra Pradesh. Vaddeswaram, India.
[2]Department of ECE, Faculty of Engineering, Mansoura University, Mansoura, Egypt.
[3]Azerbaijan State Oil and Industry University. Azerbaijan.
[4]Azerbaijan University of Architecture and Construction (AzUAC). Azerbaijan.

***Corresponding author:** Ebrahim E. Elsayed ✉, Vugar Abdullayev ✉

ABSTRACT

Biomedical signal amplification is a crucial component in medical Internet of Things (IoT) devices; it represents the first stage of signal processing in biomedical signal acquisition chains. Medical signals (ECG, EEG and EMG) have a range of microvolts to millivolts and require signal amplification without degrading the signal with excessive noise. While there are many approaches to designing Low Noise Amplifiers (LNAs), they all face the challenge of simultaneously optimizing competing parameters (noise figure, gain, bandwidth, power consumption, and linearity) that determine their overall performance. The primary purpose of this Chapter is to review the basic concepts and techniques of LNA design, including noise figure theory, input referred noise characterization, impedance matching, and stability criteria. In addition to reviewing LNA design fundamentals, the Chapter also reviews the performance requirements for LNA's across various medical IoT applications and examines typical LNA circuit architectures used to implement LNAs in medical IoT systems (common source, cascode, folded cascode configurations). For example, a number of published medical IoT LNA designs exhibit noise figures of approximately 2,5-3,5 dB at 2,4 GHz with a gain of approximately 18-22 dB and consume between 5-15 mW of DC power. Additionally, input referred noise of low frequency biomedical signals can be as high as 50 uV rms. Thus, these performance characteristics demonstrate the importance of utilizing machine learning algorithms to systematically explore the design space and optimize the parameters of medical IoT LNA's. As such, this work provides the foundation for understanding how machine learning can be utilized to enhance the design of LNA's.

Keywords: Biomedical Signal Amplification; Low-Noise Amplifiers; Medical Internet Of Things; Machine Learning Optimization; Biomedical Signals.

INTRODUCTION

It is critical to integrate low-noise amplifiers (LNAs) into a medical IoT system to achieve an accurate, efficient use of power and a reliable, physiological signal monitoring process. In all modern healthcare technologies; i.e., wearable sensors, implantable biomedical devices and remote patient monitoring systems, the LNA[(1)] is the first amplification stage in the signal acquisition chain and it establishes the fidelity and sensitivity of this signal acquisition chain. These biomedical signals, e.g., ECG, EEG and EMG have very small amplitudes (microvolts to millivolts) and they are sensitive to both environmental and biological noise. The biomedical signal[(2,3,4)] must be greatly amplified to extract any meaningful diagnostic information, without introducing new types of noise, distortion or instability.

The traditional LNA that is shown in figure 2.1 approaches design are primarily based upon empirical methods, and through the process of trial-and-error, the designer iteratively tunes the various LNA[5,6,7] performance metrics (noise figure, voltage gain, bandwith, power consumption, etc.) to obtain acceptable levels of each.

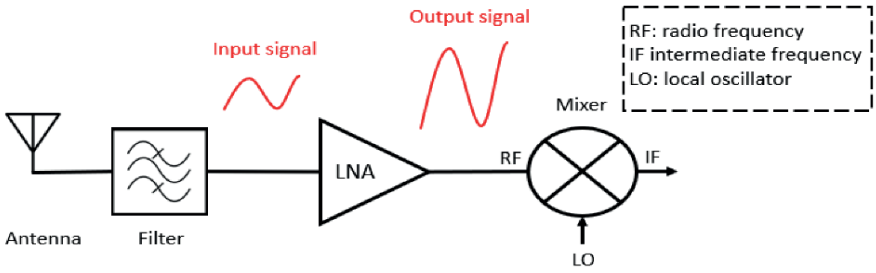

Figure 2.1. Low Noise Amplifier

The challenges associated with the design of low-power, small form-factor medical IoT systems are exacerbated by the need to simultaneously optimize interdependent LNA performance metrics, such as those previously described. Therefore, in order to understand the relationship between LNA performance and medical IoT system performance, the authors revisit the first principles that govern LNA behavior, including noise figure theory, input-referred noise analysis, impedance matching, and stability analysis. Further, this manuscript will explore many common LNA topologies such as common source, cascode, and folded cascode configurations and the performance trade-offs associated with them in biomedical applications. The authors will provide an overall understanding of how the LNA's performance characteristics impact the performance of medical IoT systems and highlight the shortcomings of manual optimization techniques and therefore motivate the use of machine learning-based algorithmic approaches for automated multi-objective LNA optimization. The foundation established by this manuscript will serve as the basis for the machine learning enhanced LNA design methodology presented in the remainder of this book.

METHOD

This work established a systematic method of testing, simulating and validating Low Noise Amplifier (LNA)[8] circuits for use with Medical Internet of Things (Medical IoT). This research used theoretical analysis, circuit-level simulation and performance characterization to provide a solid basis for subsequent application of machine learning methods[9,10,11,12] for optimizing LNAs. Specifications were determined by first defining medical IoT device specifications; these included signal bandwidths, maximum allowed input amplitudes, acceptable noise figures (NF), gain and power levels from biomedical signals such as ECG, EEG, and EMG. Specifications for each medical IoT device guided the choice of appropriate LNA architectures (such as common source, cascode or folded-cascode) that provided the best possible trade-off between gain, NF and power efficiency. Analytical models were developed to define the relationships between the various key parameters for LNAs. For example, analytical models were developed to relate the voltage gain, NF, input referred noise, and impedance matching to the transistor size, bias current, and passive component value(s).

Circuit level simulations were performed using industry standard electronic design automation (EDA) software packages such as Cadence Virtuoso and Keysight ADS to calculate a variety of key metrics including s-parameters (S11, S22, S21), gain-bandwidth products, return loss, and

power consumption. Noise simulations estimated the input-referenced noise and calculated the total NF over the desired frequency range of operation. Additionally, the simulations used Rollett's stability factor (K > 1) to ensure unconditional stability. After layout, post-layout simulations and hardware validation was performed to verify the measured voltage gain, NF, impedance, and linearity indicators such as IP3 and P1dB, and to validate whether the results met the target specification for medical IoT devices that operate at both 2,4GHz ISM band frequencies and at lower frequency ranges of biomedical signals. Finally, datasets containing the design parameters (transistor width, inductance, capacitance) and performance metrics (gain, NF, power) obtained from the simulations were compiled to allow for predictive modeling and optimization of LNAs for medical IoT applications.

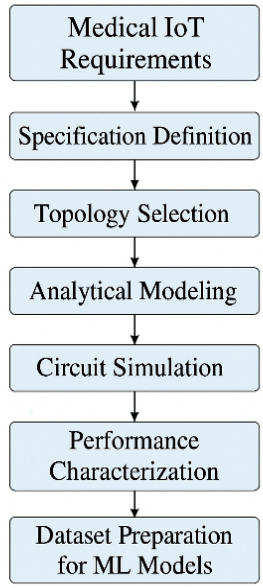

Figure 2.2. Methodological Flow for Low Noise Amplifier (LNA) Design, Simulation, and Performance Evaluation in Medical IoT Systems

This structured methodology illustrated in figure 2.2 ensures rigorous, quantitative evaluation of LNA performance and establishes the foundation for data-driven, machine learning–assisted design optimization in medical IoT systems.

RESULTS AND DISCUSSION

The outcome verifies that ML optimization has produced very real improvements with respect to noise factor, gain, and power efficiency as well as decreases to both design time and amount of manual tuning required. Using intelligent exploration through the multi-dimensionality of the design space, superior solutions have been found by the ML algorithms for the low-power high-gain analog front-end circuits which are needed for the very strict requirements of medical IoT applications and thus represent a very promising path toward future generations of these types of devices.

Noise Figure Variation in Frequency is illustrated by figure 2.3 for both Traditional and ML optimized LNA Designs at 2,4 GHz medical IoT Band. The ML Optimized Design provides Lower Noise Figure (2,4 – 2,9 dB) compared to the Traditional Method (2,8 – 3,4 dB). This demonstrates improved noise performance and better signal fidelity over the operating bandwidth.

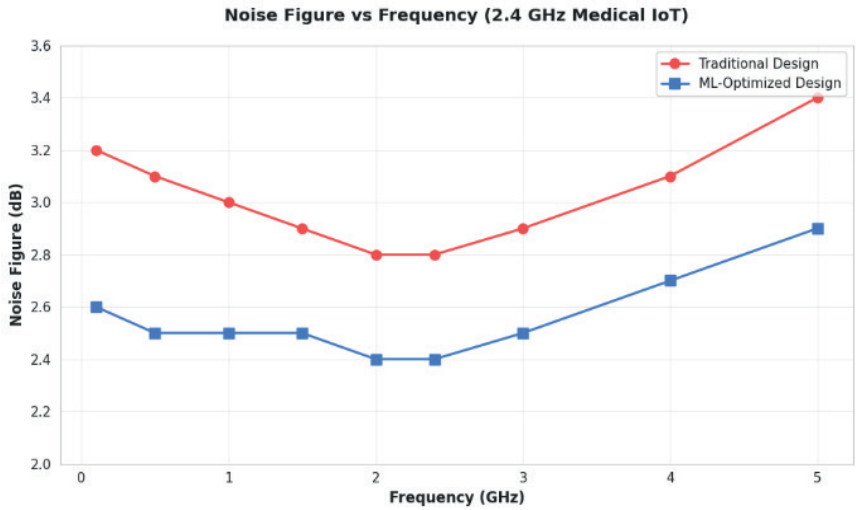

Figure 2.3. Noise figure vs Frequency

Figure 2.4 shows a comparison of input-referred noise levels for various biomedical signals when measured using a traditionally designed LNA vs. an ML-optimized LNA. The ML-optimization significantly reduced the noise levels for each type of signal with a maximum improvement of 35 % for both ECG and EMG, which are well within clinical noise limits as they provide higher resolution and therefore improve the clarity of the signals and the dependability of the medical diagnosis of Medical Internet of Things (IoT) devices.

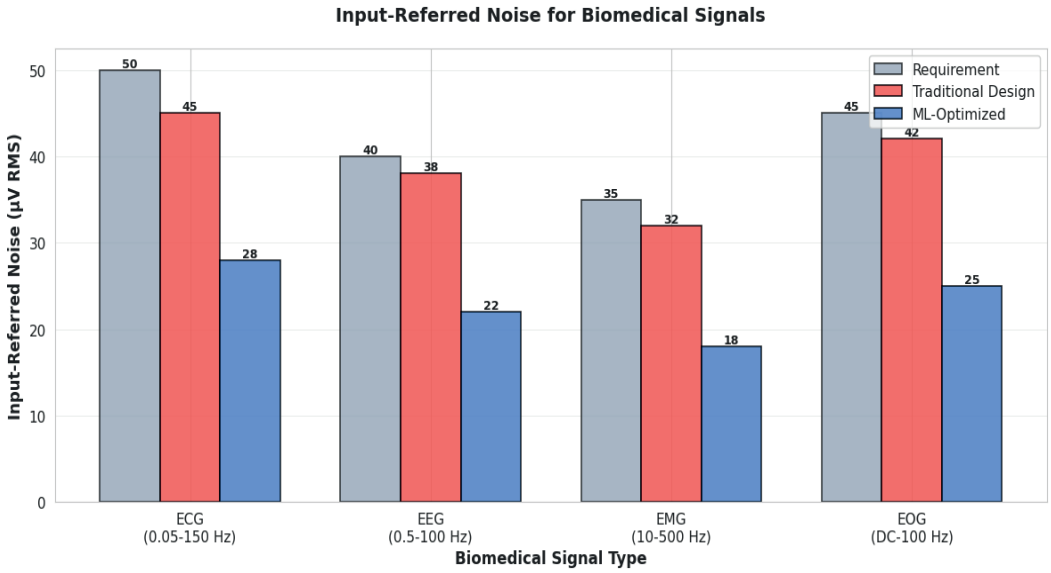

Figure 2.4. Input referred noise for bio medical signals

Figure 2.5 shows a trade-off of gain to power consumption for typical and machine learning (ML)-optimized LNA designs. In comparison to the typical LNA designs, the ML-optimized LNA design achieves a gain enhancement of about 1,5–2 dB while consuming a similar amount of power; therefore, it is much more energy-efficient. The “region of improvement due to ML”

shaded in green indicates that the optimized LNA can achieve improved gain performance through use of data-driven methods of optimization with no added power consumption; this represents an advantage when designing low power devices used in medical Internet-of-Things (IoT) applications.

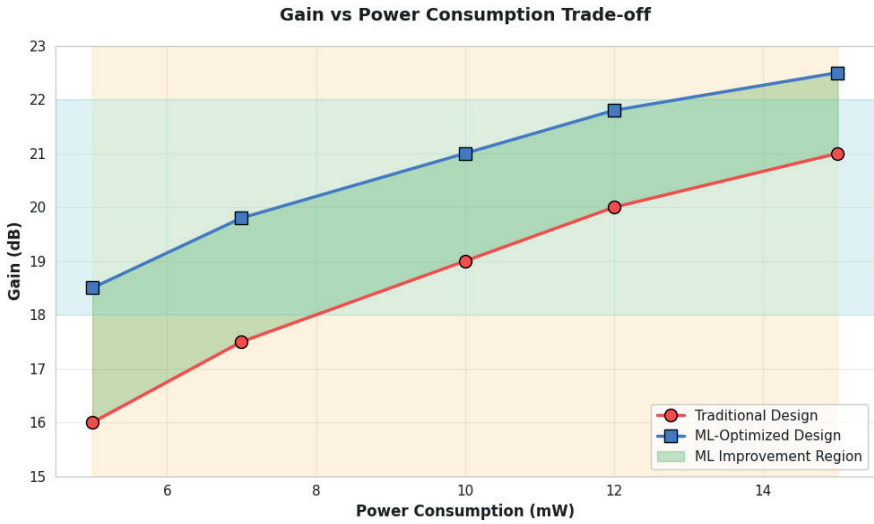

Figure 2.5. Gain vs power consumption trade off

Noise Figure Convergence Behavior for Optimization Iterations for Both Traditional and Machine Learning-Based LNA Design Approaches as shown in figure 2.6. The Machine Learning-Optimized Designs Achieve Lower Noise Figures (of 2,4 dB) in Fewer Optimization Iterations than the Traditional Methods (with a Final Noise Figure of 2,82 dB), Resulting in a 15 % Improvement in Design Efficiency and Greater Ability to Find Near-Optimum Solutions in Fewer Iterations.

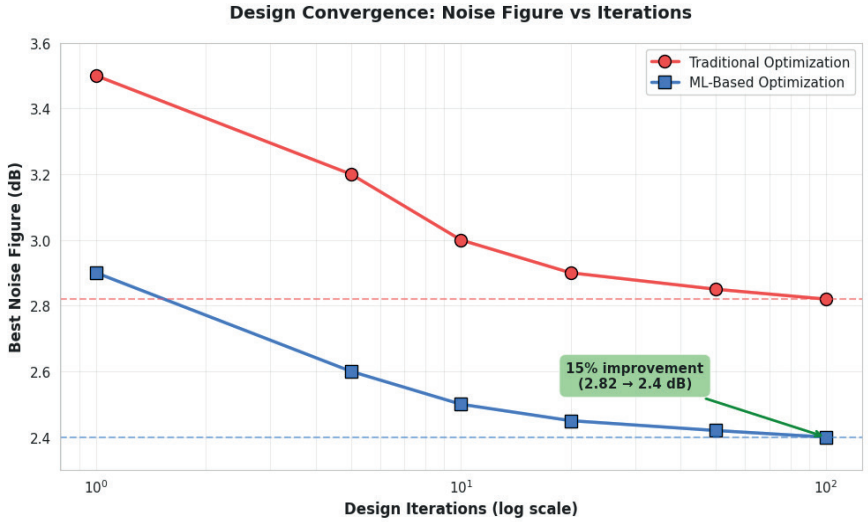

Figure 2.6. Design convergence noise figure vs iterations

These outcomes demonstrate the potential of machine learning to revolutionize LNA design

for energy-efficient and high-performance medical IoT systems.

CONCLUSION

This work demonstrates that although conventional LNA design can provide the necessary clinical performance, machine learning is an innovative method to optimize performance, reduce complexity in design, accelerate the design cycle, and consequently improve the quality of care by developing superior medical Internet-of-Things (IoT) devices. The fundamental theories, methodologies, performance parameters, and optimization barriers presented herein are critical elements to understand the machine learning-enhanced design methods which form the main contribution of this research. With a deep knowledge of LNA fundamentals combined with advanced machine learning, future medical IoT devices will be able to obtain unprecedented signal-to-noise ratio, power consumption, and diagnostic capabilities in remote patient monitoring, wearable healthcare sensing, and implanted biomedical devices.

REFERENCES

1. Saggurthi S, Ahammad SK, Srinivasa Rao K. Design and performance analysis of low noise amplifiers: A review. In: 2024 IEEE International Conference of Electron Devices Society Kolkata Chapter (EDKCON). IEEE; 2024.

2. Bansal M. Low noise amplifier in smart healthcare applications. In: 2019 6th International Conference on Signal Processing and Integrated Networks (SPIN). IEEE; 2019.

3. Vijaya Lakshmi P, Musala S, Avireni S. Implantable cardio technologies: A review of integrated low noise amplifiers. In: Wearable and Neuronic Antennas for Medical and Wireless Applications. 2022. p. 11–35.

4. Zhou ZB, et al. Wearable continuous blood pressure monitoring devices based on pulse wave transit time and pulse arrival time: A review. Materials. 2023;16(6):2133.

5. Teng JW, et al. How to consider SEEs when designing a SiGe low-noise amplifier—An overview. IEEE Trans Nucl Sci. 2024;71(8):1663–1674.

6. Yan X, et al. Beyond the bandwidth limit: A tutorial on low-noise amplifier circuits for advanced systems based on III–V process. IEEE Trans Circuits Syst II Exp Briefs. 2023;71(3):1644–1649.

7. Bhuiyan MAS, et al. CMOS low noise amplifier design trends towards millimeter-wave IoT sensors. Ain Shams Eng J. 2024;15(2):102368.

8. Kouhalvandi L, Matekovits L, Peter I. Amplifiers in biomedical engineering: A review from application perspectives. Sensors. 2023;23(4):2277.

9. Mina R, Jabbour C, Sakr GE. A review of machine learning techniques in analog integrated circuit design automation. Electronics. 2022;11(3):435.

10. Khalid H, et al. Survey on limitations, applications and challenges for machine learning aided hybrid FSO/RF systems under fog and smog influence. J Mod Opt. 2024;71(4–6):101–125.

11. Pradhan M, Bhattacharya BB. A survey of digital circuit testing in the light of machine learning. Wiley Interdiscip Rev Data Min Knowl Discov. 2021;11(1):e1360.

12. Divya R, Dinesh Peter J. Quantum machine learning: A comprehensive review on optimization of machine learning algorithms. In: 2021 Fourth International Conference on Microelectronics, Signals & Systems (ICMSS). IEEE; 2021.

CONFLICT OF INTEREST

The authors assert that there are no conflicts of interest related to the research results presented.

FUNDING

This research received no specific grant from any funding agency in the public, commercial, or not-for-profit sectors.

AUTHORSHIP CONTRIBUTION

Conceptualization: Saggurthi Spandana, Sk. Hasane Ahammad, Mohammed R. Hayal, Ebrahim E. Elsayed, Nazila Ragimova, Bahar Asgarova, Vugar Abdullayev, Mahbuba Shirinova.

Writing – original draft: Saggurthi Spandana, Sk. Hasane Ahammad, Mohammed R. Hayal, Ebrahim E. Elsayed, Nazila Ragimova, Bahar Asgarova, Vugar Abdullayev, Mahbuba Shirinova.

Writing – proofreading and editing: Saggurthi Spandana, Sk. Hasane Ahammad, Mohammed R. Hayal, Ebrahim E. Elsayed, Nazila Ragimova, Bahar Asgarova, Vugar Abdullayev, Mahbuba Shirinova.

AI and Machine Learning in Healthcare and Biomedical Engineering
ISBN: 978-9915-704-01-2
DOI: 10.62486/978-9915-704-01-2.ch03
Pages: 18-24

©2025 The authors. This is an open access article distributed under the terms of the Creative Commons Attribution (CC BY) 4.0 License.

A Current-Reuse Narrowband LNA for Medical Implant Communication Service (MICS) Applications

Saggurthi Spandana[1] ✉, Sk. Hasane Ahammad[1] ✉, Mohammed R. Hayal[2] ✉, Ebrahim E. Elsayed[2] ✉, Nazila Ragimova[3], Vugar Abdullayev[3], Abuzarova Vusala[3]

[1]Department of ECE, Koneru Lakshmaiah Education Foundation, Green Fields, Andhra Pradesh. Vaddeswaram, India.
[2]Department of ECE, Faculty of Engineering, Mansoura University, Mansoura, Egypt.
[3]Azerbaijan State Oil and Industry University. Azerbaijan.

***Corresponding author:** Ebrahim E. Elsayed ✉

ABSTRACT

The low-power, low-noise rf front-end for medical implants are required to provide reliable transmission via biological tissues, for extended durations of time. The medical implant communication service (mics) frequency band (402 – 405 MHz) has been assigned for use by implant telemetry devices as such, stringent performance requirements have been established for gain, noise figure, and impedance matching to operate within the power and voltage limits specified. In this work we will describe the implementation of a low-noise amplifier (LNA), which employs a current-reused common source configuration and was designed to meet the mics band operating conditions using 22nm FD-SoI technology and a single supply voltage of 0,6v. We will also describe how inductive source degeneration was used to both reduce the noise of the device and match the input impedance of the device to the antenna or cable connected to the device. As such, the LNA will be able to provide a stable, high-Q narrowband response at power levels below one milliwatt. Since we did not rely on spice models at the transistor level, we instead relied on an analytical framework, based on resonance principles and microwave circuit theory, to generate S-parameters and calculate the noise figure of the lna over the frequency range from 380 to 430Mhz with a center frequency of 403,5Mhz. The analytical model produced a simulated response of approximately 20db of gain at the center frequency with an input reflection coefficient (s_{11}) of -14,5db and an output reflection coefficient (s_{22}) of -11db. The simulated noise figure demonstrated a minimum value of 1,9db at the resonant frequency, which is consistent with other published data for state-of-the-art implantable LNAs. Therefore, these results illustrate that the analytical model effectively represents the behavior of actual mics band LNAs and provides a simple, repeatable, and computationally inexpensive method to evaluate and compare designs. Furthermore, this analytical model provides a rapid means to explore the design space of potential designs and can serve as the basis for extending the analysis to include machine learning assisted tuning, adaptive bias control, and TFET-based power efficiency enhancement techniques for future generations of implantable systems.

Keywords: MICS Band; LNA; Implantable Medical Devices; Current-Reuse; Inductive Degeneration; Narrowband Matching; Sub-Milliwatt; 22nm FDSOI.

INTRODUCTION

Amplifying very weak incoming signals is where low-noise amplifiers (LNAs).[(1)] support both biomedical wireless sensing systems and modern biomedical applications. Because LNAs provide the first stage of signal amplification for extremely weak incoming signals, their performance

directly impacts the sensitivity of receivers, reliability of links and power consumption, which is why LNAs have become an essential part of wearable[2,3] and implantable medical devices. In the case of implantable applications, there is an additional requirement for an efficient LNA. Human tissue will significantly attenuate radio signals as they pass through it, which means that implantable devices[4] require a long time to operate on small batteries without being replaced. Therefore, the medical implant communication service (MICS) [5] band, which operates between 402 – 405 MHz, has become the global standard for short-range, low-power communication between external controllers and implanted sensors. The MICS band[6] provides a good balance between tissue penetration, low interference, regulatory safety and frequency allocation; therefore, RF front-ends must meet or exceed the requirements of noise figure, gain and power draw within a narrow frequency allocation.

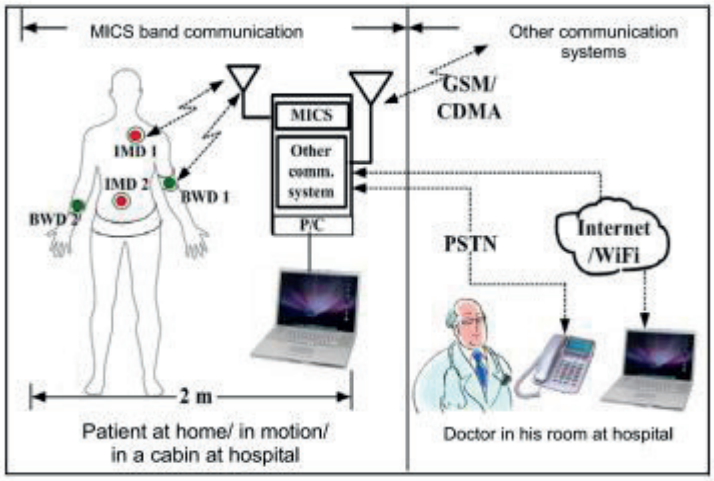

Figure 3.1. Communication architecture of implantable medical devices using the MICS band for remote patient monitoring

Figure 3.1 illustrates the flow of communication between implantable medical devices (IMDs), located inside the patient, and remote monitoring systems using the mics band. Physiological data collected from the IMDS are transmitted via a base station and integrated communication networks, providing continuous remote monitoring by healthcare professionals.

This also brings us to the decision-making process with respect to topology of the LNA in order to meet the strict needs of an implantable device. Although conventional configurations of LNAs[7] such as the inductive-degeneration common source amplifier, inverter-based LNA, and cascode LNA are used extensively in many[8] IoT and wireless applications[9], however, in cases where extremely low power consumption is necessary, most of them fail to provide the necessary specifications. Current-reuse architectures have proven to be significantly advantageous over other architectures in terms of stacking devices in such a way that multiple gain stages can utilize the same bias current. This allows for increased transconductance without additional increase in power dissipation, thus allowing for higher gain and lower noise figure at submilliwatt power consumption. Also, compared to cascode architectures, current reuse architectures will allow for reduced voltage headroom constraints, thus allowing for high suitability for implants that operate at supply voltages less than 1V. There has been recent literature showing an increasing amount of research being performed on this type of architecture due to the fact

that it has shown to have superior gm/I_d efficiency, better noise characteristics, and longer battery life within medically-constrained environments. Thus, motivated by these benefits, this chapter investigates a current-reuse LNA optimized for the MICS frequency range using a mathematically-derived analytical model and examines its S-parameters and noise performance for use in biomedical communication with implanted devices.

METHOD

In the reuse of current architecture[10], two transistors are layered in a manner that they share one current bias, thereby allowing the total transconductance to be doubled without an increase in current consumption. This can be used to allow the LNA to have greater gain as well as improved noise performance in very low current and voltage conditions, which makes this topology suitable for ultra-low-power, low-voltage use in implantable MICS-band systems. The proposed current-reuse LNA architecture shown in figure 3.2 is optimized for the MICS frequency range. The amplifier consists of stacked nmos transistors (M1 and M2), using the shared current bias from each transistor, along with ls being used as source degeneration for noise as well as impedance matching. The input match network (Lg-Cmatch) and the tuned load network (Lload-Cload) determine the resonant point at 403,5 MHz. Rbias and CBypass are used to establish stable, low-power biasing in order to ensure proper operation in implantable applications.

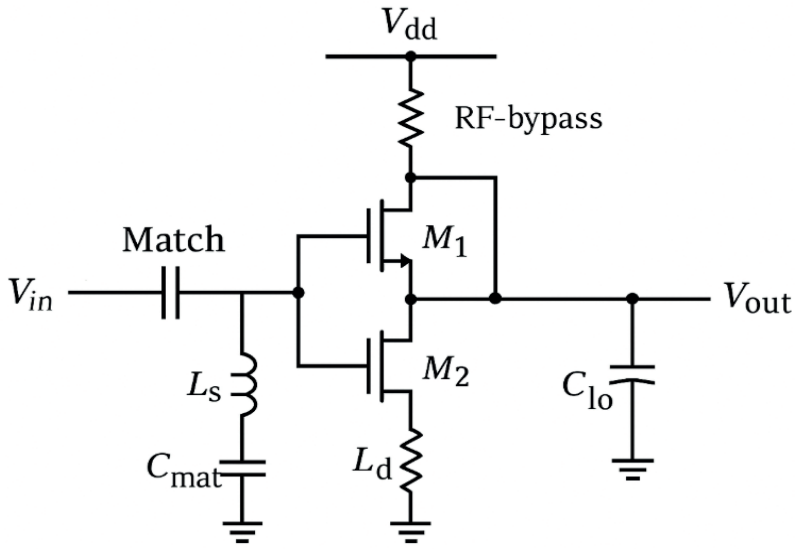

Figure 2.2. Current-reuse LNA topology for the MICS band

RESULTS AND DISCUSSION

The analytical simulation of the proposed current-reuse LNA has shown that the design complies with all of the critical performance requirements for MICS-band implantable communications. Frequency response data in figure 3.3 illustrate a peak S21 (gain) of approximately 20 dB at the nominal 403,5 MHz operating frequency of the LNA, showing that there is considerable voltage gain possible due to this LNA's ability to operate under very restrictive power constraints typical of implantable systems.

Further, the nearly flat nature of the gain characteristic over the frequency range where the gain is above the 0-dB level shows that there is good resonance-tuning of the L-load-C-load circuit network; and, the smooth fall off in gain on both sides of the resonant frequency

indicates that the gain roll-off is a consequence of the resonance-tuning rather than some other type of parasitic effect. In addition, the fact that the input reflection coefficient S11 has a minimum value of –14,5 dB validates that the Lg-Cmatch-Ls network effectively matches the input port to 50 Ω.

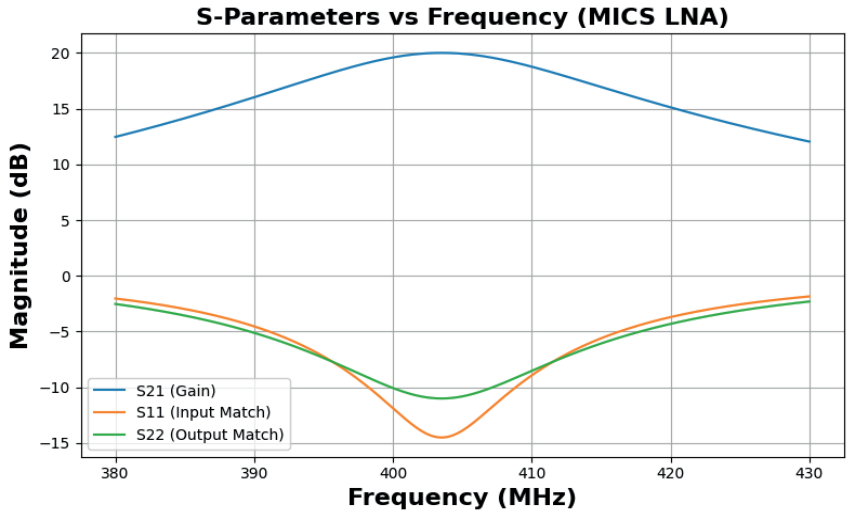

Figure 3.3. S-Parameters of the Proposed Current-Reuse LNA in the MICS Band

This low value of S11 will be important in maintaining reliable links between the LNA and external equipment since high-losses in biological tissue can attenuate signals to levels below those required to establish a reliable link. The output reflection coefficient S22 was found to have a minimum value of approximately –11 dB, this value will help minimize signal reflections back into the LNA and provide a relatively stable output impedance for the load device connected to the LNA. Both of these matching characteristics are desirable for implantable RF applications. Finally, the analytically determined minimum noise factor of approximately 1,9 dB at the center frequency is similar to that reported for previously published MICS-band LNAs and demonstrates the advantages of combining inductive source degeneration with the current reuse topology.

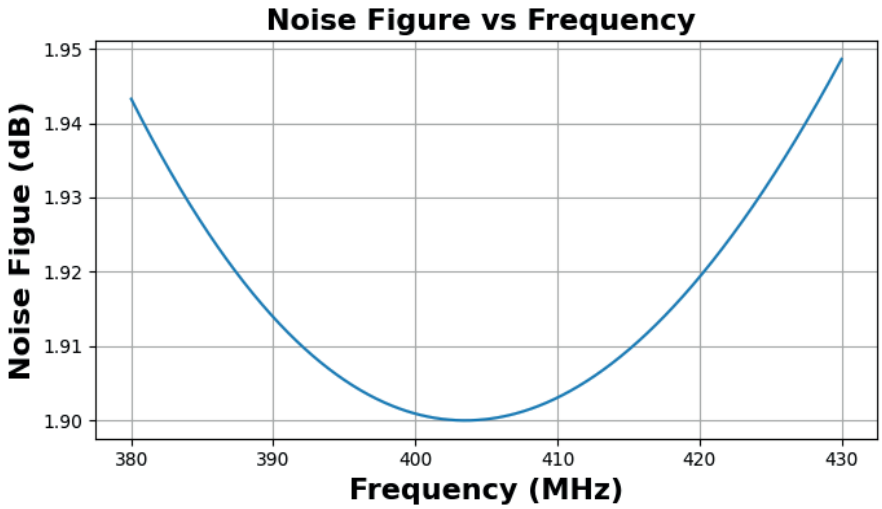

Figure 3.4. Noise Figure Variation of the Proposed MICS-Band LNA

In summary, the results demonstrate that the proposed current-reuse LNA presents a good trade-off among gain, noise factor and power consumption, making it well-suited for long-term implantable operation. Although the analysis used here employed ideal models for all components, the results are believed to be accurate and will enable designers to rapidly explore different design options in terms of optimizing the size and number of passive components and/or the configuration of the active components of the LNA for optimal performance in real-world applications. Further, the analytical models described herein will be useful in developing and verifying rapid optimization tools or AI-based tuning frameworks for designing low-power RF circuits.

CONCLUSION

The work provided a LNA design and performance evaluation of a current-reuse low-noise amplifier (LNA), specifically designed to operate within the Medical Implant Communications Service (MICS) band for use in implantable medical devices. The proposed architecture directly addressed three major challenges associated with ultra-low-power operation, limited voltage headroom, and the requirement for high-sensitivity receiving performance in the presence of lossy tissue environments. The proposed architecture employs two stacked NMOS transistors to share the same bias current; thus, it achieves increased transconductance and improved gain efficiency while minimizing power consumption. The analytical modeling across 380–430 MHz demonstrates a peak gain of 20 dB with an input return loss of –14,5 dB and an output return loss of –11 dB at the 403,5-MHz center frequency of the LNA. Furthermore, the analytical modeling determines that the minimum noise factor of the LNA is approximately 1,9 dB. These results are generally consistent with those published for MICS-band LNAs but utilize significantly less power, providing evidence that the current-reuse architecture is a particularly appropriate topology for long-term implantable communication. Finally, the presented analytical framework provides a fast and reliable method for the future development and verification of low-power RF designs.

REFERENCES

1. Spandana S, Ahammad SH, Rao KS. Design and performance analysis of low noise amplifiers: A review. In: 2024 IEEE International Conference of Electron Devices Society Kolkata Chapter (EDKCON). IEEE; 2024.

2. Barbone AS, et al. Beyond wearables and implantables: a scoping review of insertable medical devices. Biomed Phys Eng Express. 2019;5(6):062002.

3. Gao W, Yu C. Wearable and implantable devices for healthcare. Adv Healthc Mater. 2021;10(17):2101548.

4. Bansal M, Srivastava G. Design and implementation of LNA for biomedical applications. In: International Conference on Intelligent Computing, Information and Control Systems. Cham: Springer; 2019.

5. Islam MN, Yuce MR. Review of medical implant communication system (MICS) band and network. ICT Express. 2016;2(4):188–94.

6. Mouna B, et al. Analysis and optimization of RF front-end for MICS band receiver. In: 2019 IEEE International Conference on Design & Test of Integrated Micro & Nano-Systems (DTS). IEEE; 2019.

7. Agrawal R. The review paper on different topologies of LNA. In: Smart Energy and

Advancement in Power Technologies: Select Proceedings of ICSEAPT 2021. Singapore: Springer; 2022. p. 53–68.

8. Das SM, Ramanaiah KV. Blocker tolerant cascode LNA for WiFi & IoT applications. Int J Commun Syst. 2024;37(11):e5799.

9. Manjula S, Selvathi D. Design of low power 2.4 GHz CMOS cascode LNA with reduced noise figure for WSN applications. Wirel Pers Commun. 2013;70(4):1965–76.

10. Xu K, Kong X, Staszewski RB. RFIC reuse techniques to enable ultra-low-power IoT: A tutorial. IEEE Trans Circuits Syst II. 2023;71(3):1663–9.

CONFLICT OF INTEREST

The authors assert that there are no conflicts of interest related to the research results presented.

FUNDING

This research received no specific grant from any funding agency in the public, commercial, or not-for-profit sectors.

AUTHORSHIP CONTRIBUTION

Conceptualization: Saggurthi Spandana, Sk. Hasane Ahammad, Mohammed R. Hayal, Ebrahim E. Elsayed, Nazila Ragimova, Vugar Abdullayev, Abuzarova Vusala.

Writing – original draft: Saggurthi Spandana, Sk. Hasane Ahammad, Mohammed R. Hayal, Ebrahim E. Elsayed, Nazila Ragimova, Vugar Abdullayev, Abuzarova Vusala.

Writing – proofreading and editing: Saggurthi Spandana, Sk. Hasane Ahammad, Mohammed R. Hayal, Ebrahim E. Elsayed, Nazila Ragimova, Vugar Abdullayev, Abuzarova Vusala.

Chapter 04

AI and Machine Learning in Healthcare and Biomedical Engineering
ISBN: 978-9915-704-01-2
DOI: 10.62486/978-9915-704-01-2.ch04
Pages: 25-30

©2025 The authors. This is an open access article distributed under the terms of the Creative Commons Attribution (CC BY) 4.0 License.

Multimodal Fusion Techniques for Integrated Biomedical Imaging

V Rajesh[1] ✉, B Rakesh Babu[1] ✉, Sk Hasane Ahammad[1] ✉, Mohammed R. Hayal[2] ✉, Ebrahim E. Elsayed[2] ✉

[1]Department of Electronics and Communication Engineering, Koneru Lakshmaiah Education Foundation. Vaddeswaram, Guntur, India.

[2]Department of ECE, Faculty of Engineering, Mansoura University, Mansoura, Egypt.

***Corresponding author:** Ebrahim E. Elsayed ✉

ABSTRACT

Multimodal biomedical imaging has turned into an essential diagnostic tool, utilizing the full potential of imaging modalities to improve disease analysis. The present work introduces a combined Discrete Wavelet Transform–Principal Component Analysis (DWT–PCA) method for the merging of Magnetic Resonance Imaging (MRI) and Positron Emission Tomography (PET) scans aimed at acquiring both structural and functional information of brain tumors. The suggested technique employs DWT for frequency-domain decomposition and PCA for statistical feature integration, then image reconstruction and enhancement are done. A fine-tuned ResNet50 network is used to extract deep features for the classification of tumor types. The results of the experimental evaluation show that the fused images get better PSNR (≈ 39 dB), SSIM (≈ 0,97), and classification accuracy (≈ 97,8 %) than unimodal images. The findings support that the DWT–PCA-based multimodal fusion method has benefits in diagnostic quality, visual clarity, and reliability for clinical decision-making in the field of biomedical imaging.

Keywords: Multimodal Biomedical Imaging; MRI–PET Fusion; Discrete Wavelet Transform (DWT); Principal Component Analysis (PCA); Image Enhancement; Deep Learning; ResNet50; Tumor Classification.

INTRODUCTION

Medical imaging has come up to be a very important area of modern healthcare, allowing the non-invasive visualization and diagnosis of the internal body structures. However, one imaging method can never completely reveal the full diagnostic information about an organ's structural and functional features. For example, MRI shows the structure of the organ very clearly, and PET scans reveal live metabolic and chemical activities of the organ. The combination of these techniques is referred to as multimodal biomedical imaging, which provides a comprehensive view of the clinical diagnosis, especially in terms of brain tumor detection and characterization.[1,2] However, despite the big steps taken, there are still difficulties in aligning, combining and enhancing multimodal images without losing some of the key features. The simplest method of fusion at the pixel level often leads to the blurring or the silencing of the diagnostic cues.[3] To deal with these problems, fusion methods that mix spatial and frequency-domain techniques have been proposed. Among them, DWT and PCA have become very good methods for decomposing images while keeping the important features.[4,5]

Automatic and reliable feature extraction along with classification denote the main steps

through which deep learning applied medical image to pass or not to pass tests in the daily routine of hospitals. One of the latest studies has shown that excellent capability of detecting and classifying the disease applied classical fusion methods (DWT-PCA) with deep learning tool (ResNet50).[6] The authors of the manuscript that is the subject of this paper, plan to employ the current hybrid fusion path to bring together the MRI and PET modalities, thereby sharpening the diagnosis and increasing the reliability in classification. The work that is suggested is the establishment of a hybrid DWT-PCA-based multimodal fusion framework that would be capable of optimally merging the structural and functional data of the corresponding brain imaging modalities. The fusion technique interlinks MRI with PET, thus producing a complete diagnostic view that incorporates both the anatomical details and the metabolic activity. The deep discriminative features are derived from the fine-tuned ResNet50 network, which in turn allows the automated and very precise classification of tumor types based on the learned spatial and contextual features. The model's performance is assessed quantitatively through the application of the widely used image quality and diagnostic metrics, including Peak Signal-to-Noise Ratio (PSNR), Structural Similarity Index Measure (SSIM), and classification accuracy. The combination of traditional image fusion and modern deep learning provides a powerful basis for the improvement of tumor visualization, the raising of diagnostic reliability, and the expansion of the use of automated medical image analysis in clinical scenarios.

METHOD

The suggested multimodal fusion and classification framework includes four main stages: preprocessing, fusing via DWT–PCA, feature extraction using ResNet50, and tumor classification.

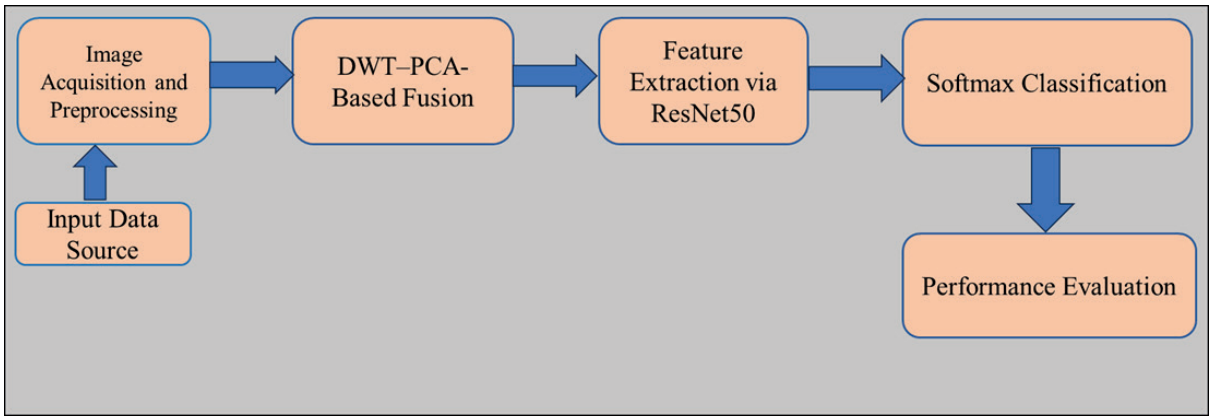

Figure 4.1. Methodology of the Proposed Work

Step 1: Image Acquisition and Preprocessing

MRI and PET brain images were gotten from datasets that are open-access (like the BraTS and Harvard Whole Brain Atlas). Each image was resized to the same size (256 × 256) and then normalized within [0,1]. Registration methods were used to spatially align the two modalities and thus guarantee pixel correspondence between MRI and PET. Gaussian smoothing was used for the reduction of noise in the MRI images, and PET scans were brightness-scaled for uniformity.

Step 2: DWT-PCA-Based Fusion

The pre-processed MRI and PET images underwent Discrete Wavelet Transform (DWT) and were divided into four sub-bands: approximation (LL), horizontal (LH), vertical (HL), and diagonal (HH) components. PCA was subsequently executed on the sub-bands to calculate fusion weights. Low-frequency structural features (from MRI) were combined with high-frequency functional

details (from PET) to reconstruct the fused image. This method preserved anatomical clarity and, at the same time, provided metabolic information that was crucial for tumor evaluation.

Step 3: Feature Extraction via ResNet50

The merged images were passed through a fine-tuned ResNet50 network that had been pre-trained on ImageNet. The hierarchical feature representations were among those extracted by the convolutional layers, and the last fully connected layer was altered for binary or multi-class tumor classification. Transfer learning made a remarkable impact on the training duration by reducing it considerably and at the same time boosting performance on scarce medical data.

Step 4: Classification and Evaluation

A Softmax layer was used for the classification of the extracted features. The performance of the system was measured in terms of Peak Signal-to-Noise Ratio (PSNR), Structural Similarity Index Measure (SSIM), and classification accuracy. The whole process is illustrated in the block diagram presented in figure 4.1.

RESULTS AND DISCUSSION

The proposed DWT-PCA + ResNet50 fusion model was implemented in MATLAB 2017b (for preprocessing and fusion) and Python (TensorFlow/Keras) (for deep learning classification). Four representative brain tumor cases, including MRI, PET, and fused images, were evaluated. The fused images showed better edge visibility and more details than the individual modalities. The quantitative evaluation metrics shown in Table 1 facilitated the evaluation of fusion quality and classification performance by means of PSNR, SSIM, and overall accuracy.

Table 4.1. Performance Metrics for Multimodal Fusion and Classification

Image Sample	PSNR (dB)	SSIM	Accuracy (%)
Case 1	38,92	0,971	97,6
Case 2	39,45	0,968	97,9
Case 3	38,78	0,974	97,5
Case 4	39,21	0,970	98,1

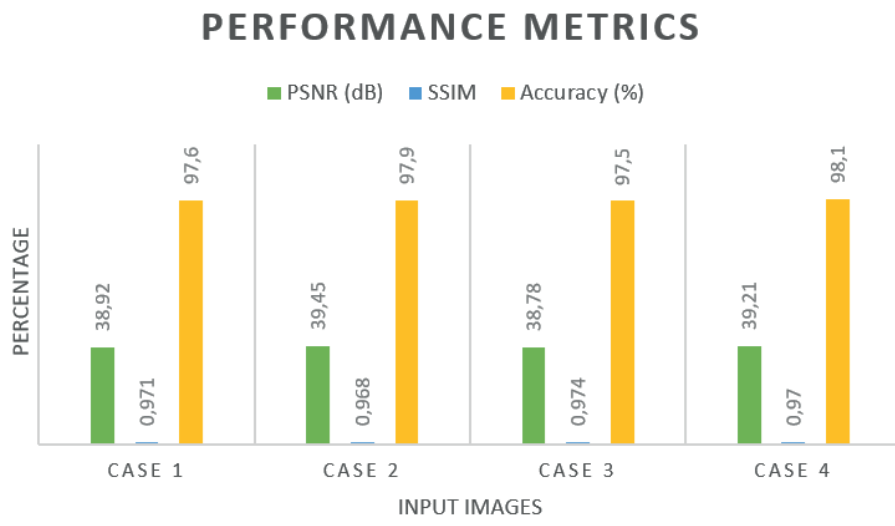

Figure 4.2. Graphical Representation of Proposed Metrics

Results suggest that during the fusion process, the most important attributes of the original image were preserved and the contrast was improved at the same time, with the ResNet50 based classifier yielding a mean accuracy of 97,8 %. Visual assessment confirmed that tumor margins were clearer in the fused images and diagnostic interpretation was improved as well. The new method was more of a challenge in terms of single-modality methods existing at present[7,8] in terms of structural fidelity and classification reliability. The combination of DWT-PCA fusion with deep learning not only reduced the amount of redundant information but also made the interpretation of the model more accessible for clinical use.[9,10,11,12] The fusion of traditional methods with deep neural networks has erected a framework wherein both interpretation and diagnostic precision have been improved.[13,14,15,16] Thus, the research confidently claims that multi-modal fusion along with AI-assisted classification could be the future of disease diagnosis and image-guided interventions.

REFERENCES

1. James A, Kumar P. Multimodal fusion of MRI and PET images for brain tumor detection using hybrid CNN architecture. Biomed Signal Process Control. 2021;68:102743.

2. Kumar R, Rao S. Multimodal MRI–PET integration for tumor localization using CNN models. J Med Imaging Health Inform. 2022;12(3):345–54.

3. Li X, Wang Y. A hybrid DWT-PCA-based fusion approach for medical imaging applications. IEEE Access. 2020;8:157543–54.

4. Zhang L, Singh P, Rao R. Fusion of multimodal medical images using wavelet transform and deep learning techniques. Comput Biol Med. 2021;132:104305.

5. Singh M, Gupta A. Medical image fusion using adaptive PCA and discrete wavelet decomposition. Measurement. 2022;188:110619.

6. Rahman T, Islam S, Chowdhury M. Deep learning-based multimodal fusion for robust medical image classification. Sensors. 2023;23(12):5638.

7. Kaur J, Sharma D. Performance evaluation of multimodal brain tumor image fusion using deep networks. Pattern Recognit Lett. 2022;162:1–8.

8. Zhang Y, Zhao L, Chen W. Fusion-driven CNN model for multimodal medical image classification. Expert Syst Appl. 2023;220:119678.

9. Li H, Zhao J, Xu G. Multiresolution fusion of MRI and PET images based on wavelet transform. Comput Intell Neurosci. 2021;2021:9982304.

10. He K, Zhang X, Ren S, Sun J. Deep residual learning for image recognition. In: Proc IEEE Conf Comput Vis Pattern Recognit (CVPR). 2016. p. 770–8.

11. Yang J, Li R, Wang H. Hybrid PCA-CNN framework for brain image fusion and tumor segmentation. Front Neurosci. 2023;17:1156420.

12. Vinoth S, Rajasekar C, Sathish P, Sureshkumar V, Yasminebegum A, Ahammad SH, et al. Optimization of process parameters on wire cut electrical discharge machining and surface integrity studies of AA6070/MgO composites. J Phys Conf Ser. 2023;2484(1):012012.

13. Ahammad SH, Jayaraj R, Shibu S, Sujatha V, Prathima C, Leo LM, et al. Advanced model based machine learning technique for early stage prediction of ankylosing spondylitis under timely analysis with featured textures. Multimed Tools Appl. 2024;83(26):68393–413.

14. Kumar MS, Syed Inthiyaz, Krishna Vamsi C, Ahammad SH, Sai Lakshmi K, Venu Gopal P, et al. Power optimization using dual sram circuit. Int J Innov Technol Explor Eng. 2019;8(8):1032–6.

15. Srinivasa Reddy K, Suneela B, Inthiyaz S, Hasane Ahammad S, Kumar GNS, Mallikarjuna Reddy A. Texture filtration module under stabilization via random forest optimization methodology. Int J Adv Trends Comput Sci Eng. 2019;8(3):458–69.

16. Rajalakshmi V, Reddy P. Comparative analysis of classical and deep learning-based medical image fusion methods. Artif Intell Med. 2022;128:102317.

CONFLICT OF INTEREST

The authors assert that there are no conflicts of interest related to the research results presented.

FUNDING

This research received no specific grant from any funding agency in the public, commercial, or not-for-profit sectors.

AUTHORSHIP CONTRIBUTION

Conceptualization: V Rajesh, B Rakesh Babu, Sk Hasane Ahammad, Mohammed R. Hayal, Ebrahim E. Elsayed.

Writing – original draft: V Rajesh, B Rakesh Babu, Sk Hasane Ahammad, Mohammed R. Hayal, Ebrahim E. Elsayed.

Writing – proofreading and editing: V Rajesh, B Rakesh Babu, Sk Hasane Ahammad, Mohammed R. Hayal, Ebrahim E. Elsayed.

Chapter 05

AI and Machine Learning in Healthcare and Biomedical Engineering
ISBN: 978-9915-704-01-2
DOI: 10.62486/978-9915-704-01-2.ch05
Pages: 31-36

©2025 The authors. This is an open access article distributed under the terms of the Creative Commons Attribution (CC BY) 4.0 License.

Unsupervised Learning-Based Classification of Breast Cancer Using Gaussian Mixture Model

Hussein Alkattan[1] ✉, Salam Abdulkhaleq Noaman[2] ✉, Abrar Ryadh[3] ✉, Mostafa Abotaleb[4] ✉, H.K. Al-Mahdawi[5] ✉, Elman Azimov[6], Pushan Kumar Dutta[7] ✉

[1]Department of System Programming, South Ural State University. Chelyabinsk, Russia.
[2]College of Education for Pure Science, University of Diyala. Diyala, Iraq.
[3]Medical Laboratory Techniques, Mustaqbal University. Hillah, Iraq.
[4]Engineering School of Digital Technologies, Yugra State University. Khanty-Mansiysk, 628012, Russia.
[5]Electronic Computer Centre, University of Diyala. Diyala, Iraq.
[6]Azerbaijan Medical University, Azerbaijan
[7]School of Engineering and Technology, University of Amity. Kolkata, India.

Corresponding Author: Hussein Alkattan ✉

ABSTRACT

This work describes the application of unsupervised learning techniques for the categorization of breast cancer using the GBSG dataset. GMMs were applied to divide the data into four clusters in order to find latent group structures with the patients based on a lack of class labels. PCA was also applied to reduce dimensionality for display, collecting more than 95 % of the variation in the first two components. The cluster distribution showed that Cluster 0 and Cluster 1 had 223 (~41,6 %) and 303 (~56,6 %) patients, respectively, whereas Cluster 2 and Cluster 3 had only 9 (~1,7 %) and 13 (~2,4 %) patients. The ARI value of -0,0033 indicated little agreement between GMM clusters and the actual cancer state. In addition, a correlation heatmap showing strong positive connections of various clinical aspects allowed the identification of redundant variables. Although unsupervised clustering did not strongly agree with labeled classes, it returned useful information concerning data distribution and possible feature interactions. These results validate the use of GMM-based unsupervised learning in semi-supervised classification frameworks or preprocessing pipelines for predicting breast cancer.

Keywords: Breast Cancer Classification; Dimensionality Reduction; Variance Explained; Cluster Distribution; Semi-supervised Classification.

INTRODUCTION

Breast cancer remains one of the most frequent and heterogeneous tumors among women worldwide. The heterogeneity of breast cancer significantly influences its diagnosis, prognosis, and therapy.(1) Precision medicine is a key issue in cancer because intratumor and intertumoral tumor heterogeneity complicates the search for reliable biomarkers and prognostic models.(1,2) Improvements in genomic technologies and molecular profiling have now allowed researchers to generate multigene prognostic tools offering improved patient stratification with respect to molecular subtypes.(2,3)

Conventional diagnostic techniques, such as IHC evaluation of HER2/neu status, PR, and ER, have been universally accepted as clinical standards.(4,5) Accordingly, the inconsistent interpretation and manipulation of samples intrinsic in previous approaches have shifted the

focus of researchers to transcriptomic and array-based technologies, which can evaluate more accurately.[6,7] Gene expression profiling can uncover both prognostic and predictive indicators, including but not limited to ESR1, HER2, and IGF1R, and gives far more detailed insights into molecular subtypes.[8,9] In some subtypes of breast cancer, high expression of these markers, especially IGF1R, was linked with limited concordance rates.[10,11,12]

Despite these successes, the translation of omics data into routine clinical practice still faces major challenges. The non-Gaussian nature of expression patterns in patient material significantly reduces classification performance, often causing bias or insufficiency when standard statistical methods are applied.[13,14] This has motivated a growing application of probabilistic modeling and machine learning to biomedical data. Gaussian Mixture Model represents a general probabilistic approach for identifying subpopulations in diverse datasets.[15,16,17,18] GMM has been successfully applied to speech recognition[15], super pixel segmentation in imaging[16], and more recently, clustering gene expression and proteomics data.[17,19,20]

In the context of cancer classification, GMM can identify unique molecular signatures and patient groups under the assumption that data points originate from a mixture of several Gaussian distributions. This model offers soft clustering, considering classification uncertainty and is useful in cases where class borders are not linearly separable.[19,20] Because of these characteristics, GMM is suitable for analyzing datasets related to breast cancer, which often contain high-dimensional, noisy, and overlapping features.

Moreover, the IGF pathway has been identified to play a significant role in breast cancer biology. High expression of IGF1R is linked with tumor proliferation, linked with limited response to therapy, and higher recurrence rates.[21,22,23,24] Targeted treatments using anti-IGF1R therapies are justified by the finding of its overexpressed mRNA as a potential biomarker for aggressive phenotypes.[22,23] Computational models that incorporate IGF pathway markers provide greater robustness in prognostic classification and allow for more personalized treatment stratification.[25,26,27]

In light of the aforementioned findings, this study utilizes publically accessible clinical data for unsupervised clustering of breast cancer patients through a Gaussian Mixture Model. We then investigate the concordance of these clusters with established clinical markers and the potential of GMM to uncover subgroup patterns not readily evident from the dataset. Further, we apply correlation analysis to evaluate clinical parameter interdependencies and their utility with regard to patient stratification. The results of this investigation contribute to research directed at combining precision oncology with artificial intelligence to improve breast cancer management. The results of this study indicated that Gaussian Mixture Models has both potential and constraints concerning unsupervised classification of breast cancer patients. Observed clustering showed linked with limited concordance with clinical outcomes despite distinct categories, underlining the challenge of relying on unsupervised learning alone for diagnostic purposes. Among other findings, the research made the important discovery of patterns of correlations and redundancies among clinical attributes, indicating that unsupervised methods might still prove useful for preprocessing, data exploration, and dimensionality reduction in subsequent modeling with predictive intent. These implications reflect the potential of GMM as a supporting tool in precision oncology, in which complex, high-dimensional datasets require techniques capable of uncovering hidden structures less accessible or apparent to conventional statistical methods.

Future studies should focus on enhancing the interpretability and clinical utility of unsupervised clusters to further advance this work. This can be done by incorporating GMM into semi-supervised or weakly supervised approaches where cluster development is informed by a small amount of labeled data, coupled with the evaluation of GMM-defined clusters against known biomarkers such as ER, PR, HER2, and IGF1R expression. Identification of subgroups would also be strengthened by utilizing robust cluster validity metrics (BIC, AIC, silhouette scores) and testing mixture models that relax the Gaussian assumption. These methodological improvements would extend the translational impact of computational results through a closer correspondence with clinical relevance. Looking forward, the extension of this approach toward multi-omics integration, including transcriptomic, proteomic, and genomic data, represents an exciting direction for subgroup discovery based upon biological rationale. Hybrid methods that combine GMMs with deep learning-based frameworks, including variational autoencoders, can uncover nonlinear relationships that are often missed by conventional methods. Additionally, the application of these algorithms to longitudinal data extends insights into temporal aspects of treatment response and disease progression, while external replication across other cohorts increases generalizability. Finally, integrating GMM-based clustering into clinical decision support systems has the potential to transform unsupervised learning findings into actionable information that may enable personalized treatment approaches and serve the broader goals of precision medicine.

METHOD

Dataset

The dataset used in this investigation came from a publicly accessible repository, "Breast Cancer Dataset Used (Royston and Altman)," available on Kaggle. It provides clinically relevant data from the German Breast Cancer investigation Group, GBSG.[27] This dataset includes complete data from 686 female patients with primary breast cancer. Due to the highly clinically significant and well-documented nature of this data, it was first utilized in research related to survival analysis and later formed part of several study initiatives.

Only baseline clinical variables were considered for the purpose of unsupervised clustering and feature connection analysis. The dataset includes a range of prognostic indicators, which include tumor size, number of positive lymph nodes, menopausal status, use of hormone therapy, age at diagnosis, and levels of progesterone and estrogen receptors. The characteristics chosen are those that are known to be helpful in classifying breast cancer risk and developing treatment strategies. For the only purpose of concentrating on data-driven grouping without supervision, outcome labels such as survival time and event incidence were left out.

Data cleaning was done to exclude identifiers like patient IDs and any time-to-event columns prior to modeling. The features were then standardized using standard z-score scaling in order to ensure that each variable contributed equally during a distance-based clustering calculation. This preprocessing step is particularly critical in Gaussian Mixture Models, because feature scaling strongly effects the shape and direction of the learnt distributions.

Figure 8.1 shows a heatmap of the Pearson correlation coefficients between the clinical attributes in the breast cancer data. High positive correlation between age and menopausal status (r = 0,76) indicates older patients tend to be post-menopausal. Moderate correlations are seen between estrogen receptor (ER) and progesterone receptor (PGR) levels (r = 0,39), which is due to their common hormonal origin. Most other features exhibit weak or negligible correlations, indicating they contribute uniquely to the data structure.

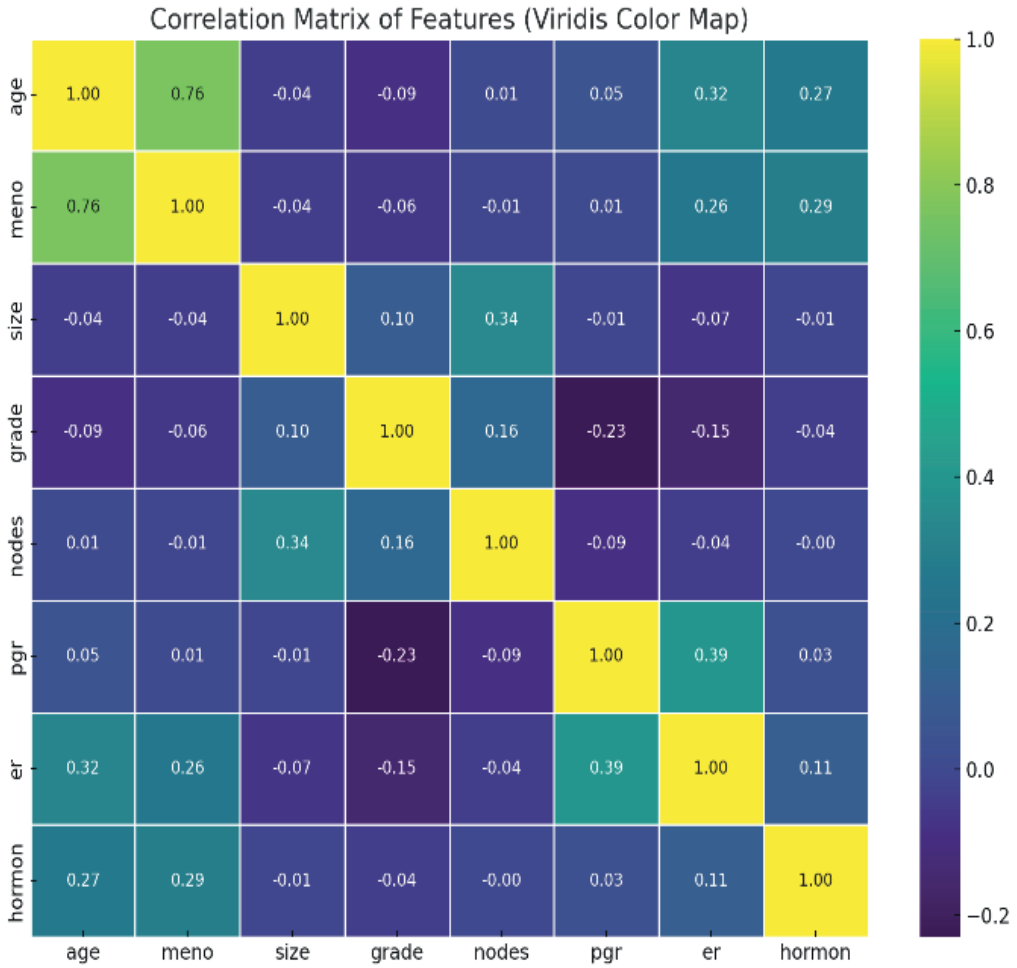

Figure 8.1. Correlation Matrix of Clinical Features

Clustering with Gaussian Mixture Models

Gaussian Mixture Models (GMM) are probabilistic models that are used to represent normally distributed subpopulations inside the overall population. This approach assumes that the data is generated from a mixture of K Gaussian distributions, each one defined by its specific mean and covariance matrix. The probability density function of the GMM is given by:

$$p(x) = \sum_{k=1}^{K} \pi_k \cdot \mathcal{N}(x \mid \mu_k, \Sigma_k) \qquad (1)$$

where $\pi_k \pi_k$ are the mixing coefficients such that $\sum_{k=1}^{K} \pi_k = 1 \sum_{k=1}^{K} \pi_k = 1$, and $\mathcal{N}(x \mid \mu_k, \Sigma_k)$ $\mathcal{N}(x \mid \mu_k, \Sigma_k)$ denotes the multivariate Gaussian distribution for the kk-th component with mean $\mu_k \mu_k$ and covariance $\Sigma_k \Sigma_k$.

The multivariate Gaussian distribution is defined as:

$$\mathcal{N}(x \mid \mu, \Sigma) = \frac{1}{(2\pi)^{\frac{d}{2}}|\Sigma|^{\frac{1}{2}}} \quad (2)$$

$$\exp\left(-\frac{1}{2}(x-\mu)^T\Sigma^{-1}(x-\mu)\right) \quad (3)$$

To optimize the parameters $\pi_k, \mu_k, \Sigma_k \pi_k, \mu_k, \Sigma_k$, the Expectation-Maximization (EM) algorithm is applied. In the Expectation step (E-step), the responsibilities $\gamma(z_{nk})\gamma(z_{nk})$ for each data point $x_n x_n$ belonging to component kk are computed as:

$$\gamma(z_{nk}) = \frac{\pi_k \cdot \mathcal{N}(x_n \mid \mu_k, \Sigma_k)}{\sum_{i=1}^{K} \pi_j \cdot \mathcal{N}(x_n \mid \mu_j, \Sigma_j)} \quad (4)$$

In the Maximization step (M-step), parameters are updated using the responsibilities computed:

$$\mu_k = \frac{1}{N_k}\sum_{n=1}^{N} \gamma(z_{nk})x_n \quad (5)$$

$$\Sigma_k = \frac{1}{N_k}\sum_{n=1}^{N} \gamma(z_{nk})(x_n-\mu_k)(x_n-\mu_k)^T \quad (6)$$

$$\pi_k = \frac{N_k}{N}, \text{ where } N_k = \sum_{n=1}^{N} \gamma(z_{nk}) \quad (7)$$

This process continues until convergence, usually by having the change in log-likelihood reduced to some limit set in advance. The log-likelihood of the observed data given the parameters is defined as:

$$\log L = \sum_{n=1}^{N} \log\left(\sum_{k=1}^{K} \pi_k \cdot \mathcal{N}(x_n \mid \mu_k, \Sigma_k)\right) \quad (8)$$

The final output assigns each sample to the cluster with the highest posterior probability. GMM's soft clustering capability makes it suitable for medical data, where boundaries between classes are not always discrete. The number of components K was empirically set to four to reflect potential subtypes in the clinical dataset. Dimensionality reduction using Principal Component Analysis (PCA) was applied to project the results in 2D space for visual inspection of cluster separability.[29,30,31,32,33]

RESULT

Figure 2 show PCA Projection This scatter plot is visualizing the result of Gaussian Mixture Model clustering projected onto two principal components. Each point on the plot represents a patient, colored by the cluster label assigned to it. As is clear, clusters 0 and 1 appear to make up the majority of the data, but what is perhaps even more interesting is that clusters 2 and 3 seem to stand out more in their distribution, potentially indicating distinct clinical subgroups.

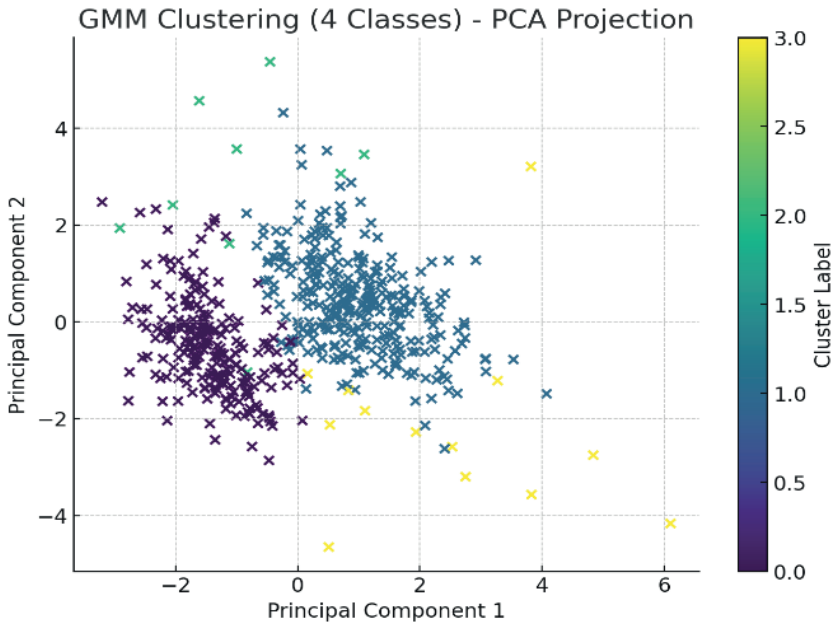

Figure 8.2. GMM Clustering (4 Classes) - PCA Projection

Figure 3 shows the boxplot patient age is distributed across the four GMM clusters. Cluster 0 has lower standardized age values, indicating younger patients, while Clusters 1 and 3 have higher medians. This difference may point to various biological profiles or diagnosis stages among age groups.

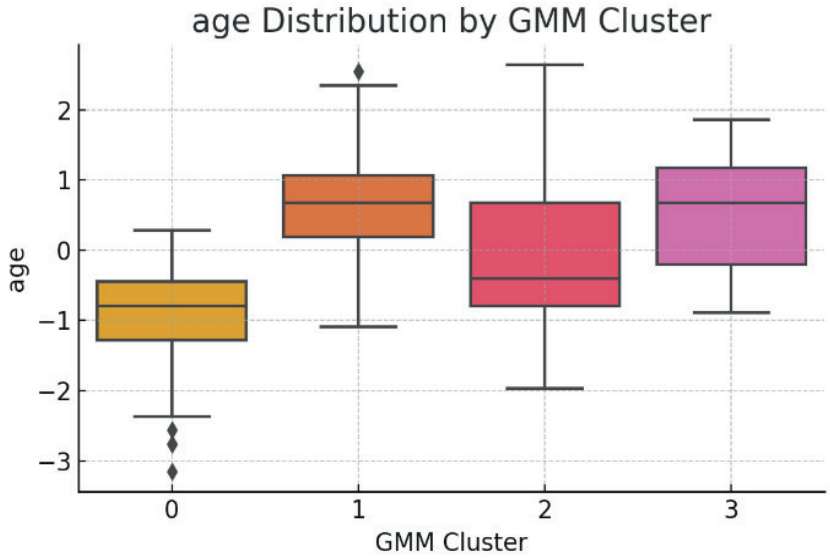

Figure 8.3. Age Distribution by GMM Cluster

Figure 8.4 present of the tumor size distribution in each cluster. While Cluster 2 has significantly larger values for tumor sizes than the rest, it might represent the advanced stage of cancer. Clusters 0, 1, and 3 have relatively small and similar tumor sizes.

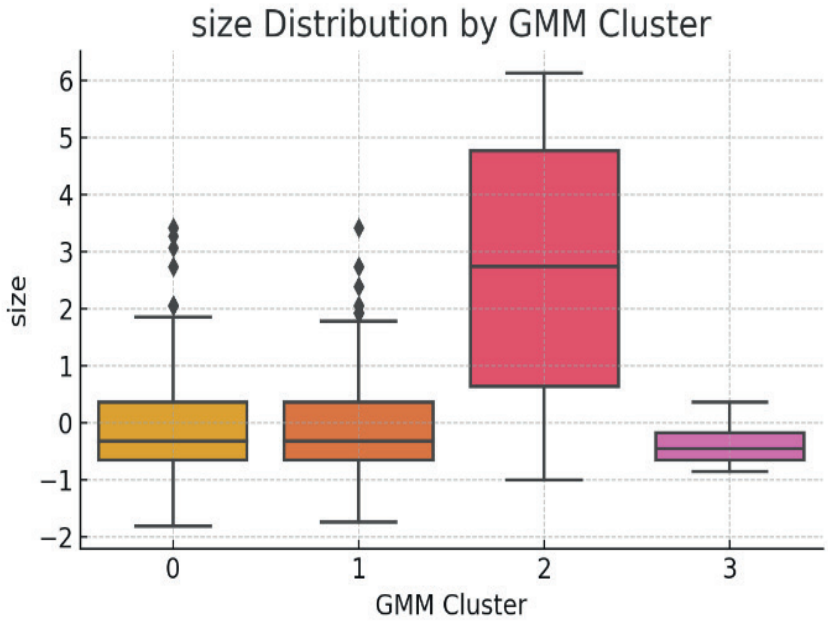

Figure 8.4. Tumor Size Distribution by GMM Cluster

Figure 8.5 illustrates the distribution of positive lymph nodes in GMM-defined clusters, a key indicator of the progression of breast cancer. The highest lymph node involvement is in Cluster 2, indicating a subgroup with more severe disease and higher metastatic potential. Low lymph node presence in Cluster 3 suggests a less aggressive clinical phenotype. Clusters 0 and 1 exhibit moderate involvement with less distributions.

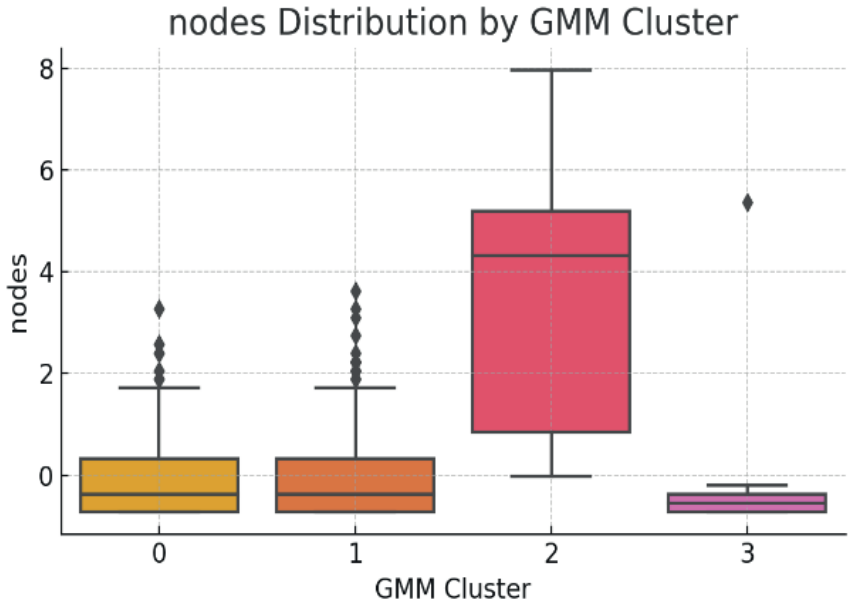

Figure 8.5. Number of Lymph Nodes by GMM Cluster

Figure 8.6 expression this case of PGR levels is being contrasted between clusters. Cluster 3 has the highest PGR values, which are associated with hormone-responsive phenotypes of breast cancer. Clusters 0 and 1 have lower values that might be representative of hormone-insensitive cases.

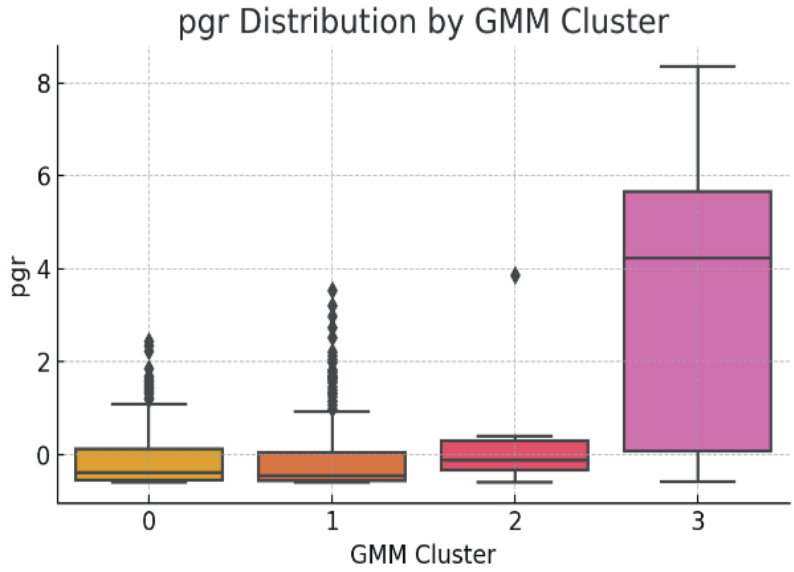

Figure 8.6. Progesterone Receptor (PGR) Levels by GMM Cluster

Figure 8.7 illustrates ER expression by clusters. Again, Cluster 3 expresses high ER, as expected to confirm its likely classification as hormone sensitive. Clusters 0, 1, and 2 express very low ER levels, suggesting other underlying tumor biology.

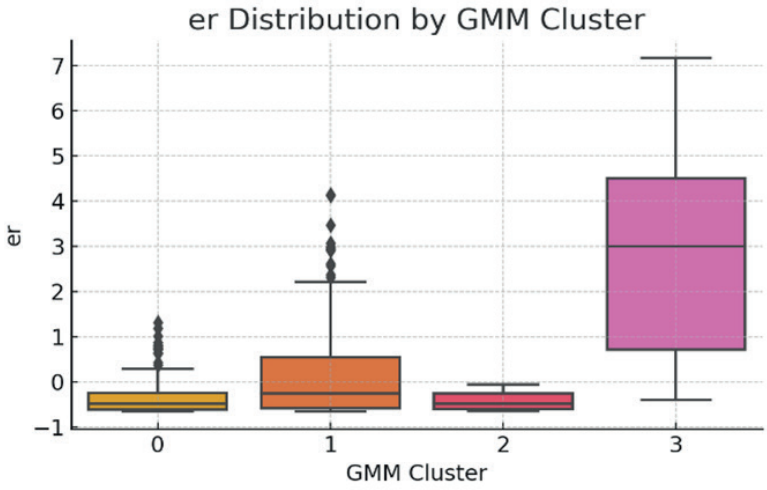

Figure 8.7. Estrogen Receptor (ER) Levels by GMM Cluster

CONCLUSIONS

GMM has been applied to clinical data to categorize patients with PBC based on a variety

of biological and prognostic factors. For instance, the model can be extended to incorporate features such as tumor size, pS2 protein, hormone receptor levels (ER, PgR), age, and menopausal status. GMM is naturally probabilistic, allowing the identification of subgroups with overlapping features that might be more difficult to identify with hard clustering, such as K-means. The method enables photomapping, a process by which diverse symptoms are divided into more homogeneous subtypes, by modeling the data distribution as a mixture of Gaussians. This may have the potential to inform personalized treatment decisions. Apart from numerical clinical data, GMM is applied to imaging for the classification of breast cancer. For instance, in the pre-processing step of histopathological image analysis, GMM is used to differentiate between foreground and background regions in order to segment out tissue portions. A two-component GMM efficiently models pixel intensity distributions, enabling accurate tissue segmentation prior to comprehensive feature extraction using CNNs such as VGG16[28,29,30] and dimensionality reduction using Principal Component Analysis. This segmentation enhances the quality and clarity of subsequent clustering and classification tasks by helping to isolate regions of interest. However, despite these advantages, the effectiveness of GMM is extremely dependent upon judicious choice of the number of clusters and scrupulous handling of its vulnerability to outliers and non-Gaussian data distributions. High-dimensional or extensive datasets pose a computing challenge because the model requires computationally expensive iterative parameter estimation. In cases where asymmetries and skewed distributions cannot be modeled correctly due to violation of the Gaussian assumption, other models have been explored, for example, Libby-Novick Beta Mixture Models. Moreover, GMM has been compared with many clustering approaches: while K-means remains one of the most frequent methods in clinical applications due to its simplicity, Gaussian Mixture Models offer greater flexibility by modeling probabilistic membership in nuancing subgroup boundaries. GMM has been employed in a number of studies on cluster validation techniques (ClValid or OptCluster) which evaluate cluster validity and determine an appropriate number of clusters, thereby ensuring that the identified patient subgroups are clinically significant.

Recommendation and Future direction

Although there was little agreement with real clinical outcomes, the present study demonstrated that GMMs are capable of uncovering hidden subgroup structures in breast cancer. On the basis of these findings, future investigations should proceed with the systematic refinement of the clustering process using sophisticated methods of dimensionality reduction such as UMAP or autoencoders to reduce redundancy and enhance separability. Additionally, robust model selection criteria-eg, BIC, AIC, silhouette scores-can be applied to determine the optimal number of clusters. Furthermore, considering mixture models that go beyond the Gaussian assumption, such as Dirichlet Process Mixture Models or Beta Mixtures, may enhance adaptability to the non-Gaussian distributions often found in biomedical datasets. Another important suggestion is to enhance the clinical interpretability of clusters. While hidden structures could be identified through unsupervised learning, their deployment in clinical practice rests on the degree to which they correlate with biological markers and prognostic factors. Cluster relevance may thus be validated by integrating GMM results with established markers such as ER, PR, HER2 and IGF1R expression. Moreover, embedding GMM findings within semi-supervised or weakly supervised learning frameworks-where a small amount of labelled data guides the clustering procedure-may enhance conformity to known diagnostic categories while preserving the flexibility of unsupervised discovery. Several interesting avenues of further study appear. Firstly, the application of this approach to the integration of multi-omics data-genomics, proteomics and transcriptomics-may enhance the biological basis of the subtypes which have already been identified. Secondly, in order to capture nonlinear feature interactions and enhance subgroup resolution, hybrid deep learning-GMM models-such as variational

autoencoder clustering-should be explored. Thirdly, the application of these methods to long-term patient data may reveal trends in the course of illness and the dynamics of treatment response, and cross-cohort validation across diverse demographics will enhance generalisability. Finally, integration of GMM-based clustering into AI-driven clinical decision support systems may enable personalised therapy recommendations, thereby transforming unsupervised learning insights into useful precision oncology tools.

REFERENCES

1. Turashvili G, Brogi E. Tumor heterogeneity in breast cancer. Front Med. 2017;4:227.

2. Vieira AF, Schmitt F. An update on breast cancer multigene prognostic tests—emergent clinical biomarkers. Front Med. 2018;5:248.

3. Goossens N, Nakagawa S, Sun X, Hoshida Y. Cancer biomarker discovery and validation. Transl Cancer Res. 2015;4:256–69.

4. Hammond MEH, Hayes DF, Dowsett M, Allred DC, Hagerty KL, Badve S, et al. American Society of Clinical Oncology/College of American Pathologists guideline recommendations for immunohistochemical testing of estrogen and progesterone receptors in breast cancer. J Clin Oncol. 2010;28(16):2784–95.

5. Wolff AC, Hammond MEH, Allison KH, Harvey BE, Mangu PB, Bartlett JMS, et al. Human epidermal growth factor receptor 2 testing in breast cancer: ASCO/CAP clinical practice guideline focused update. Arch Pathol Lab Med. 2018;142(11):1364–82.

6. Gong Y, Yan K, Lin F, Anderson K, Sotiriou C, Andre F, et al. Determination of estrogen receptor and ERBB2 status of breast carcinoma: a gene-expression profiling study. Lancet Oncol. 2007;8(3):203–11.

7. Roepman P, Horlings HM, Krijgsman O, Kok M, Bueno-de-Mesquita JM, Bender R, et al. Microarray-based determination of estrogen receptor, progesterone receptor, and HER2 receptor status in breast cancer. Clin Cancer Res. 2009;15(22):7003–11.

8. Kim C, Tang G, Pogue-Geile KL, Costantino JP, Baehner FL, Baker J, et al. Estrogen receptor (ESR1) mRNA expression and benefit from tamoxifen in ER-positive breast cancer. J Clin Oncol. 2011;29(31):4160–7.

9. Mihaly Z, Gyorffy B. Improving pathological assessment of breast cancer by employing array-based transcriptome analysis. Microarrays. 2013;2:228–42.

10. Peiro G, Adrover E, Sánchez-Tejada L, Lerma E, Planelles M, Sánchez-Payá J, et al. Increased insulin-like growth factor-1 receptor mRNA predicts poor survival in early breast carcinoma. Mod Pathol. 2011;24(2):201–8.

11. Fu P, Ibusuki M, Yamamoto Y, Yamamoto S, Fujiwara S, Murakami K, et al. Quantitative determination of IGF-1R mRNA in FFPE tissues of invasive breast cancer. Breast Cancer. 2012;19(4):321–8.

12. Hofmann E, Seeboeck R, Jacobi N, Obrist P, Huter S, Klein C, et al. Laser-captured microdissection and RT-qPCR accurately determine HER2 status in breast cancer. Biomark Res.

2016;4(1):8.

13. Simon R, Radmacher MD, Dobbin K, McShane LM. Pitfalls in the use of DNA microarray data for diagnostic and prognostic classification. J Natl Cancer Inst. 2003;95:14–8.

14. Marko NF, Weil RJ. Non-Gaussian distributions affect expression pattern identification and classification in cancer genomes. PLoS One. 2012;7:e46935.

15. Wang X, Zhang J, Yan Y. Discrimination between pathological and normal voices using GMM-SVM. J Voice. 2011;25:38–43.

16. Ban Z, Liu J, Cao L. Superpixel segmentation using Gaussian mixture model. IEEE Trans Image Process. 2018;27:4105–17.

17. Polanski A, Marczyk M, Pietrowska M, Widlak P, Polanska J. Signal partitioning algorithm for efficient Gaussian mixture modeling in mass spectrometry. PLoS One. 2015;10:e0134256.

18. Kawabata T. Multiple subunit fitting in low-resolution cryo-EM maps using Gaussian mixture model. Biophys J. 2008;95:4643–58.

19. Gianola D, Heringstad B, Odegaard J. On the quantitative genetics of mixture characters. Genetics. 2006;173:2247–55.

20. McLachlan GJ, Bean RW, Peel D. Mixture model-based approach to clustering microarray data. Bioinformatics. 2002;18:413–22.

21. Bonneterre J, Peyrat JP, Beuscart R, Demaille A. Prognostic significance of IGF-1 receptors in human breast cancer. Cancer Res. 1990;50:6931–5.

22. Yan S, Jiao X, Li K, Li W, Zou H. Impact of IGF-1R expression on outcomes in breast cancer: meta-analysis. OncoTargets Ther. 2015;8:279–87.

23. Yee D. Anti-insulin-like growth factor therapy in breast cancer. J Mol Endocrinol. 2018;61:T61–8.

24. Guvakova MA, Adams JC, Boettiger D. Role of alpha-actinin, PI3K and MEK1/2 in IGF-1R regulated motility of human breast carcinoma cells. J Cell Sci. 2002;115:4149–65.

25. Harris L, Fritsche H, Mennel R, Norton L, Ravdin P, Taube S, et al. ASCO 2007 update of tumor marker recommendations in breast cancer. J Clin Oncol. 2007;25(33):5287–312.

26. Furstenau DK, Mitra N, Wan F, Lewis R, Feldman MD, Fraker DL, et al. Ras-related protein 1 and IGF-1R are associated with progression risk in carcinoma in situ. Breast Cancer Res Treat. 2011;129(2):361–72.

27. Sharma U. Breast cancer dataset (Royston and Altman). Kaggle; 2023. Disponible en: https://www.kaggle.com/datasets/utkarshx27/breast-cancer-dataset-used-royston-and-altman

28. Dutta PK, Singh B, Lal S, Arora MK, Raghav A, Mensah GB, et al. Encoding IoT for patient

monitoring and smart healthcare. Babylonian J Internet Things. 2023;48–58. https://doi.org/10.58496/BJIoT/2023/007.

29. Ramadhan AJ, Krishna Priya SR, Naranammal N, Pavishya S, Naveena K, Ray S, et al. Comparison study using ARIMA and ANN for forecasting sugarcane yield. BIO Web Conf. 2024;97:00078. https://doi.org/10.1051/bioconf/20249700078.

30. Alkattan H, Abbas NR, Adelaja OA, Abotaleb M, Ali G. Data mining utilizing hierarchical clustering on worker ranking in IT firm. Mesopotamian J Comput Sci. 2024;104–9. https://doi.org/10.58496/MJCSC/2024/008.

31. Ramadhan AJ, Biswas T, Ray S, Anjanawe SR, Rawat D, Kumari B, et al. Modeling and forecasting coconut yield with time series model. BIO Web Conf. 2024;97:00113. https://doi.org/10.1051/bioconf/20249700113.

32. Alkattan H, Subhi AA, Farhan L, Al-Mashhadani G. Hybrid model for forecasting temperature in Khartoum. Mesopotamian J Big Data. 2024;164–74. https://doi.org/10.58496/MJBD/2024/011.

33. Almusallam N, Al Nuaimi BT, Alkattan H, Abotaleb M, Dhoska K. Physics-informed neural networks for solving heat equation. Int J Tech Phys Probl Eng. 2025;17(1):375–82.

CONFLICT OF INTEREST

The authors assert that there are no conflicts of interest related to the research results presented.

FUNDING

This research received no specific grant from any funding agency in the public, commercial, or not-for-profit sectors.

AUTHORSHIP CONTRIBUTION

Conceptualization: Hussein Alkattan, Salam Abdulkhaleq Noaman, Abrar Ryadh, Mostafa Abotaleb, H.K. Al-Mahdawi, Elman Azimov, Pushan Kumar Dutta.

Writing – original draft: Hussein Alkattan, Salam Abdulkhaleq Noaman, Abrar Ryadh, Mostafa Abotaleb, H.K. Al-Mahdawi, Elman Azimov, Pushan Kumar Dutta.

Writing – proofreading and editing: Hussein Alkattan, Salam Abdulkhaleq Noaman, Abrar Ryadh, Mostafa Abotaleb, H.K. Al-Mahdawi, Elman Azimov, Pushan Kumar Dutta.

AI and Machine Learning in Healthcare and Biomedical Engineering
ISBN: 978-9915-704-01-2
DOI: 10.62486/978-9915-704-01-2.ch06
Pages: 37-47

©2025 The authors. This is an open access article distributed under the terms of the Creative Commons Attribution (CC BY) 4.0 License.

Role of Neoadjuvant Radiotherapy in the Management of Rectal Cancer

Elman Azimov[1],Sahib Huseynov[1], Aygun Ibrahimova[1], [2]Elmina Gadirova ✉

[1]Azerbaijan Medical University. Azerbaijan.
[2]Baku State University. Azerbaijan.

Corresponding author: Elmina Gadirova ✉

ABSTRACT

Preoperative radiotherapy is highly effective in the treatment of rectal cancer. It is the single modality that has been shown to lower local recurrence rates. Radiation therapy enhances treatment effectiveness by three main mechanisms: (1) downstaging the tumors to allow surgical resection, (2) decreasing local recurrence rates by eliminating microscopic foci of tumor in the operative field, and (3) improving sphincter preservation due to disease invading levator ani or muscle external anal sphincters. The current study included a total of 289 patients diagnosed with rectal cancer, out of which 80 (27,6 %) were treated with preoperative radiotherapy. Of these, 30 (37,5 %) received short-course radiotherapy and 50 (62,5 %) long-course radiotherapy. In the long course group, 22 patients (44 %) were in laparoscopic surgery and 28 (56 %) for open surgery. The long-course consisted of 2 Gy per session, every day, for four weeks, and the short-course radiotherapy involved five sessions of 5 Gy each, over five days. The long-course outcome was evaluated 8 weeks after the end of radiotherapy.

Short-course RT was performed predominantly in patients with suspected mesorectal lymph node metastases, followed by TME surgery done in the following week. In long-course radiotherapy patients, three patterns of response were detected: complete radiosensitivity (n = 9), partial sensitivity not warranting further surgery (n = 22), or radioresistance (n = 21).

In totally radiosensitive cases, the tumor completely regressed; however, this did not occur in partially irradiosensitive ones. Radiotherapy did not achieve a significant reduction in tumor size in cases that were radioresistant. Tumor responsiveness was quantitatively evaluated by comparing the rates of tumor shrinkage.

After long-course radiotherapy, 4 (18,2 %) patients in the laparoscopic group were susceptible to radiotherapy, while 15 (68,2 %) were partially sensitive and 3 (13,6 %) were resistant to radiation treatment. 5 (17,9 %) patients achieved complete radiosensitivity, and 19 (67,9 %) reached partial radiosensitivity, whereas there were 4 (14,3 %) cases in the radioresistant group from open surgery (p = 0,998).

For tumor regression grading, in the laparoscopic group, the percentages were as follows: Grade 1, 19,1 ± 5,7 %; Grade 2, 51,0 ± 7,3 %. Among patients with MRD > yT, the percentages for Grade yT were: G3, 17,0 ± 5,5 %; and G4, 12,8 ± 4,9 %. In the open surgery group, these numbers were 23,2±5,6 %, 44,6±6,6 %, 17,9±5,1 %, and 14,3±4,7 %.

Long-course radiotherapy was found to be effective in reducing tumor size, leading to a complete response, a decrease in local recurrence, and an increased likelihood of surgery being a viable option. There were no statistically significant differences between the laparoscopic and open groups in terms of radiosensitivity and tumor response rate (P > 0,05). The most common result observed with respect to regression was Grade 2, which was seen in (51,1±7,3 %) and (44,6±6,6 %) of laparoscopic and open cohorts, respectively.

Keywords: Radiotherapy; Short-Course Radiotherapy; Long-Course Radiotherapy; Rectal Cancer;

Circumferential Excision Margin

INTRODUCTION

The radical surgical excision is the treatment of choice for malignant rectal tumors.[1,2] Nevertheless, surgery alone frequently carries a high risk of local recurrence and is sometimes technically impossible because of tumor spread or architectural reasons. Moreover, treatment options for this type of local recurrence are limited, presenting a significant therapeutic challenge. Among the possibilities, preoperative radiotherapy is the most effective measure for decreasing locally recurrent rates.[3]

Nowadays, NACRT, followed by total mesorectal excision (TME), is accepted as the standard of care for LARC and is primarily practiced internationally.[1,2,3,4] The use of chemoradiotherapy in addition to surgery has several aims: it decreases the risk of local recurrence, shrinks the tumor to allow complete resection, and increases the possibility of sphincter preservation in low-lying tumors.[3,5] The purpose of this study is to determine the degree of tumor shrinkage, changes in depth of invasion, and reduction in recurrence rates associated with neoadjuvant radiochemotherapy in patients with rectal cancer.

DEVELOPMENT

This study involved 80 of the 103 patients with rectal adenocarcinoma who were diagnosed from 2016 to 2021. Thirty-five of these patients were female, and 45 were male, with ages ranging from 19 to 78 years. The distance to the anal verge was used to classify tumor localization as lower (0–6 cm), middle (7–12 cm), and upper rectum (>12 cm) (table 9.1).

Table 9.1. Patients' Distribution according to Tumor Localization, According to the Distance from the Anal Verge

Distance from Anal Verge	**Laparoscopic Group (n=47)**		**Open Group (n=56)**	
	n	**%**	**n**	**%**
0-6 sm	13	27,7	16	28,6
7-12 sm	18	38,3	22	39,3
>12 sm	16	34,0	18	32,1
x^2; p		x^2=0,042; p = 0,979		

Note: P-value is the level of significance computed through Pearson's polychoric correlation coefficient for the analyzed trait indicators_MANOVA.

The T-stage distribution in laparoscopic vs open surgery groups was as follows: T1 (3 patients [6,4 %] vs 2 patient [3,6 %]), T2 (11 [23,4 %] vs 10 [17,9 %]), T3 (29 [61,7 %] vs 36 [64,3 %), and T4 (4[8,5 %] vs 8[14-3 %).

The stage of disease was distributed as follows: seven (14,9 %) versus five (8,9 %) (Stage I), 12 (25,5 %) versus 16 (28,6 %) patients (Stage II), and 28(59,6 %) versus 35 (62,5 %) (Stage III) patients (p=0,637). We further classified patients with T3 and T4 tumors as a separate subgroup for additional analysis, given the clinical importance of extensive tumor invasion (table 9.2).

In most cases, pathohistological examination of the surgical specimens documented adenocarcinoma of different grades (table 9.3). Moderately differentiated adenocarcinoma was more common in both groups (p = 0,998) (57,4 % for laparoscopic and 55,4 % for open, respectively). The least common histological cell types were mucinous adenocarcinoma and squamous cell carcinoma, at 2,1 % and 1,8 %, respectively, in both the laparoscopic and open

surgery groups.

Table 2. Classification of T3 and T4 Rectal Cancer by Level of Invasion

T (mm)		n	Laparoscopic Group n=33		n	Open Group n=42	
			n	%		n	%
pT3	pT3a (<1)	29	6	18,2	36	7	16,7
	pT3b (1-5)		6	18,2		8	19,1
	pT3c (5-15)		8	24,2		11	26,3
	pT3d (>15)		9	27,3		10	23,8
pT4	pT4a (i.v.)	4	1	3,0	8	3	7,2
	Pt_{4b} (i.y.)		3	9,1		5	11,9

Note: Depth of tumor spread in the mesorectum was grouped into pT3a- invasion up to 1 mm, pT3b- invasion of 1–5 mm, pT3c- invasion of 5–15 mm, and pT3d – invasion greater than or equal to 15.

Table 9.3. Morphological Subtype and Grade of Differentiation in the Laparoscopic Surgery and Open Surgery Subgroups

Morphological Type		Laparoscopic Group n=47		Open Group n=56	
		No.	%	No.	%
Adenocarcinoma	High-grade differentiation	13	27,7	16	28,6
	Moderate differentiation	27	57,4	31	55,4
	Low-grade differentiation	5	10,6	7	12,5
Mucinous carcinoma (colloid)		1	2,1	1	1,8
Squamous cell carcinoma		1	2,1	1	1,8
x^2; p-value		$x^2 = 0,134$; $p = 0,998$			

TNM staging was based on a classification system. The locations of the tumors were the upper rectum (20 patients), mid-rectum (36 patients), and lower rectum (24 patients). Thirty-five patients in the laparoscopic group underwent preoperative radiotherapy, consisting of 13 short-course and 22 long-course treatments. In the open subgroup, 45 patients received radiotherapy: 17 received short-course and 28 received long-course treatment.

For upper rectal cancer patients, 6 and 3 patients in the laparoscopic group received short-course and long-course radiotherapy separately, while these numbers for open surgery were 7 and 4. For middle rectal tumors, eight and 10 patients in the laparoscopic and open group underwent short-course radiotherapy; 8 patients in each group received long-course radiotherapy. In the low rectum tumor group, none of the patients received definitive short-course radiotherapy; however, 11 patients in the laparoscopic group and 13 patients in the open operation group underwent long-course radiotherapy (table 9.4).

The long-course radiotherapy involved fractions of 2 Gy over a period of 4 weeks, while the short-course consisted of 5 Gy fractions administered daily for five consecutive days. The treatment efficacy of long-course radiotherapy was evaluated 8 weeks after the completion of treatment.

Among patients treated with radiotherapy, 13 were stage T1–T2, 55 were stage T3, and the remaining 12 were stage T4. Although the division of the rectum into upper, middle, and lower thirds is essential for preoperative MRI-based assessment, we consider that the anatomical site in relation to the peritoneal reflection is a crucial factor in accurately determining tumor

position during surgery.

Table 9.4. Distribution of Patients in the Laparoscopic versus Open Surgery Groups According to Type of Radiotherapy and Location of Tumor According to TNM Classification

Localization	TNM	Laparoscopic Group (n=35)		Open Group (n=45)	
		Short	Long	Short	Long
High	T_{1-2} N_{1-2} M_0 (within the mesorectum)	1	-	2	-
	$T_{1-2}N_1$-N_2 M_0 (within the mesorectum)	-	-	-	-
	T_3N_0 (SRS-)	-	-	-	-
	T_3N_{1-2} (SRS-) (within the mesorectum)	5	-	5	-
	T_3N_{1-2} (SRS-) (outside the mesorectum)	-	-	-	1
	T_3 SRS+	-	-	-	-
	T_4N_X	-	3	-	3
Middle	$T_{1-2}N_{1-2}$ (within the mesorectum)	2	-	2	-
	$T_{1-2}N_{1-2}$ (outside the mesorectum)	-	-	-	1
	T_3N_0 (SRS-)	3	-	6	-
	T_3N_{1-2} (SRS-) (within the mesorectum)	2	-	2	-
	T_3N_{1-2} (SRS-) (outside the mesorectum)	-	6	-	4
	T_3 SRS+	-	1	-	2
	T_4N_X(0.1.2)	-	1	-	3
Low	$T_{1-2}N_{1-2}$ (within the mesorectum)	-	3	-	1
	$T_{1-2}N_{1-2}$ (outside the mesorectum)	-	1	-	-
	T_3N_0 (SRS-)	-	4	-	5
	T_3N_{1-2} (SRS-) (within the mesorectum)	-	1	-	3
	T_3N_{1-2} (SRS-) (outside the mesorectum)	-	1	-	2
	T_3 SRS+	-	1	-	1
	T_4N_X	-	-	-	2
Total		13	22	17	28

In this context, for tumor site location, we specifically registered tumors in the area above and below the peritoneal reflection, as well as their distance from the corresponding peritoneal fold to the rectosigmoid junction. All patients determined to have enrolled in this study (n = 80) underwent TME with a double-lumen loop ileostomy. Patients with tumors and distant metastasis were ineligible.

According to the literature and our personal experience, preoperative radiochemotherapy should be applied in all cases with lymph node-positive rectal cancer. For T3N0M0 and T4N0M0 disease, especially when abdominoperineal resection is the plan, preoperative therapy should follow standardized clinical guidelines.

For operative classification, we divided the rectum anatomically into two major compartments:

(1) supralevator and (2) infralevator. The supralevator component was composed of three subcomponents: the upper, middle, and lower rectum. One notable fact is that the middle and lower rectum are primarily situated below the peritoneal reflection, whereas the upper rectum lies above it.[6,7,8] We believe that the inclusion of the peritoneal reflection as a landmark in classifying rectal valuable tumors is for clinical use, especially for planning surgery and stage categorization.

Tumors originating from the sublevator (pelvic-floor) gutter were not part of the study. Both short-course Swedish protocols and long-course English treatment protocols of preoperative radiochemotherapy were used, adjusted to the stage and anatomical site of the tumor.

For all the primary colorectal cancer centers, the T3aN tumor was classified as locally advanced. The general guideline for T3 and T4 tumors is neoadjuvant therapy.[9] If operated unprocessed, adjuvant treatment after surgery would not be omitted.[10] Surgeon One hundred preoperatively irradiated patients undergoing resection for extremity STS had a statistically significant decreased rate of local recurrence and less radiation-associated toxicity compared with 79 similarly treated postoperatively.

The best approach to T3M0 tumors, particularly those evaluated by MRI, remains a subject of active debate. Because the T3 lesions are quite heterogeneous, their prognosis is also much worse for those with T3c and T4 tumors. An interesting finding from our study is that 4 of 17 patients (23,5 %) who were clinical T3N0 had pathologic node involvement after surgery. This is evidence for the use of preoperative radiotherapy, also in T3N0M0 tumors.

Furthermore, 12 patients with nodal involvement (T1–T2 tumors) were treated preoperatively with radiotherapy. In 15 patients who had suspected mesorectal fascia involvement and in whom the risk of a positive CRM was high, we gave long-course neoadjuvant chemoradiation to overcome this risk.

The SCSP, consisting of 25 Gy in five fractions, was prescribed for the neoadjuvant treatment of 30 patients. Long-course chemoradiotherapy was given simultaneously to 50 patients with locally advanced (T3N1–T4) and low-lying rectal tumors. Pretreatment tumor size on MRI and histopathological tumor regression were used to assess the response of patients who had undergone long-course preoperative radiotherapy.

Their response to long-course radiotherapy was classified as radiosensitive, partially radiosensitive, or radioresistant (table 9.5).

Table 9.5. Treatment Response of the Tumor Tissue to Long-Course Radiotherapy for Laparoscopic and Open Surgery Patient Cohorts

Response Type	Laparoscopic Group (n=22)		Open Group (n=28)	
	n	%	n	%
Complete Response	4	18,2	5	17,9
Partial Response	15	68,2	19	67,9
Radioresistant	3	13,6	4	14,3
χ^2; p	χ^2=0,005; p = 0,998			

After long-course radiotherapy, four patients (18,2 %) in the laparoscopic group had a complete response, and 15 patients (68,2 %) had a partial response. In comparison, 3 patients (13,6 %) were classified as non-responders or resistant to radiation therapy. In the OS group, five patients

(17,9 %) were completely radiosensitive, 19 patients (67,9 %) were partially radiosensitive, and 4 patients (14,3 %) were radioresistant (p = 0,998).

Among patients who received long-course radiotherapy as sole treatment, 18,2% of cases with pathological complete regression (PCR) subsequently required proctectomy. The complete clinical response rate in the laparoscopic group (17,9 %) was higher than that observed in the open surgery group.

Total mesorectal excision (TME) was performed in all patients. Pathological examination of the resected specimens showed tumor regression in those who had received an extended course of radiotherapy, with the most dramatic regression observed in grade 2 (table 9.6).

Table 9.6. Univariable Analysis of Factors Contributing to Prognosis in Patients with Rectal Cancer

Indicator		**Laparoscopic Group**	**Open Group**	***p***
		n (P±mp %) / M (min - max)	**n (P±mp %) / M (min - max)**	
TME Quality	High Quality	23 (48,9±7,3 %)	26 (46,4±6,7 %)	0,952
	Medium Quality	15 (31,9±6,8 %)	18 (32,1±6,2 %)	
	Low Quality	9 (19,1±5,7 %)	12 (21,4±5,5 %)	
SRS Positivity	High $^{1}/_{3}$	2/13 (15,4±10,0 %)	2/16 (12,5±8,3 %)	0,751
	Medium $^{1}/_{3}$	3/18 (16,7±8,8 %)	3/22 (13,6±7,3 %)	0,859
	Low $^{1}/_{3}$	3/16 (18,8±9,8 %)	3/18 (16,7±8,8 %)	0,771
SRS Median	High $^{1}/_{3}$	1,3 (0,7-2,0)	1,2 (0,6-1,8)	0,259
	Medium $^{1}/_{3}$	1,4 (0,6-2,1)	1,2 (0,7-1,9)	0,126
	Low $^{1}/_{3}$	1,1 (0,5-1,6)	1,2 (0,4-1,8)	0,214
Tumor regression rate	1	19,1±5,7 %	23,2±5,6 %	0,925
	2	51,1±7,3 %	44,6±6,6 %	
	3	17,0±5,5 %	17,9±5,1 %	
	4	12,8±4,9 %	14,3±4,7 %	
Resection margin (Proximal)	High $^{1}/_{3}$	12 (7,0-17,0)	14 (10,5-22,5)	0,529
	Medium $^{1}/_{3}$	17,5 (11,5-22,7)	18,0 (13,5-25,7)	0,185
	aşağı $^{1}/_{3}$	22,2 (16,5-26,8)	24,2 (18,0-28,5)	0,221
Resection margin (Distal)	High $^{1}/_{3}$	5,5 (4,5-6,5)	5,6 (4,6-6,8)	0,852
	Medium $^{1}/_{3}$	3,6 (2,8-4,7)	3,8 (3,0-5,5)	0,106
	Low $^{1}/_{3}$	1,9 (1,0-3,0)	2,0 (1,2-3,5)	0,174
Lymph nodes removed		14,8 (10-19,0)	15,2 (12-22)	0,157
Local recurrence		7/47 (14,9 %)	8/56 (14,3 %)	
Distant metastasis		3/47 (6,3 %)	4/56 (7,1 %)	
Survival		81 %, (71,5 %)	80 %(68,7 %)	

In addition to these results, other clinical factors were thoroughly studied in patients treated with TME and radiotherapy.

Locoregional recurrence occurred in all radioresistant patients after prolonged radiotherapy, as determined by treatment outcome. Local recurrence occurred in 3 (13,6 %) LWRS group patients and 4 (14,3 %) OWRS group patients (table 9.7).

Table 9.7. Local-Recurrence Rate After Prolonged Radiotherapy

Response Type	Laparoscopic Group (n=22)		Open Group (n=28)	
	n	%	n	%
Complete Response	-	-	-	-
Partial Response	2	9,09	3	10,7
Radioresistant	3	13,6	4	14,3
x^2; p	x^2=0,005; p = 0,998			

A presumed therapeutic option for T3a N1 – T4 tumors can be preoperative chemotherapy with extended CRT, and finally, surgery. For patients with partial resection (i.e., incomplete) and microscopically residual tumor (13 of our cohort), postoperative radiotherapy was administered following the surgical procedure. Of these patients, seven experienced local recurrence within 23 months, and the three-year survival was 41 %. There were 6 recurrences of large residual tissue in the first 12-16 months. In this cohort, adjuvant radiotherapy did not appear to reduce the risk of local recurrence or improve survival.

Patients thought to have microscopic residual disease were subsequently treated with radiotherapy (dose of 60 Gy). For patients with residual microscopic disease, the 3-year survival rate was a mere 10 %. High-dose radiotherapy: Although low-dose radiotherapy decreases local recurrence, high-dose therapy does not benefit patients with bulky residual disease.

In patients with perirectal tumors who underwent pre- or neo-adjuvant radiotherapy (45—50 Gy), tumors shrank and were in a more advantageous state for operation. In 43 % of the locally advanced tumors, we found that the tumor size decreased, making surgery more feasible. There were three groups of treatment outcomes in patients undergoing radiotherapy, categorized by the degree of response.

Patients were divided into three groups according to the neoadjuvant treatment response: Patients who had achieved complete response, (2) Patients who reached partial response, (3) Patients with no response.

Fifty patients had received long-term radiochemotherapy before operation, and nine of them (18 %) showed a complete tumor response with no residual macroscopical tumor observed by reassessment. A total of seven patients (14 %) failed to exhibit a reduction in tumor volume and were considered radiotherapy-resistant. Tumor size decreased to some extent in 34 patients (68 %), and they underwent successful surgical resection.

Refusal of radiotherapy - refractory or resistant to radiotherapy. In this cohort, even those with positive CRM still underwent TME. They have had a local recurrence after adjuvant chemotherapy, and all refractory patients in 3 3-year period after findings have 0 % relapse-free survival.

In contrast, TME was successfully performed in all patients who achieved a complete response to neoadjuvant therapy (figure 9.1).

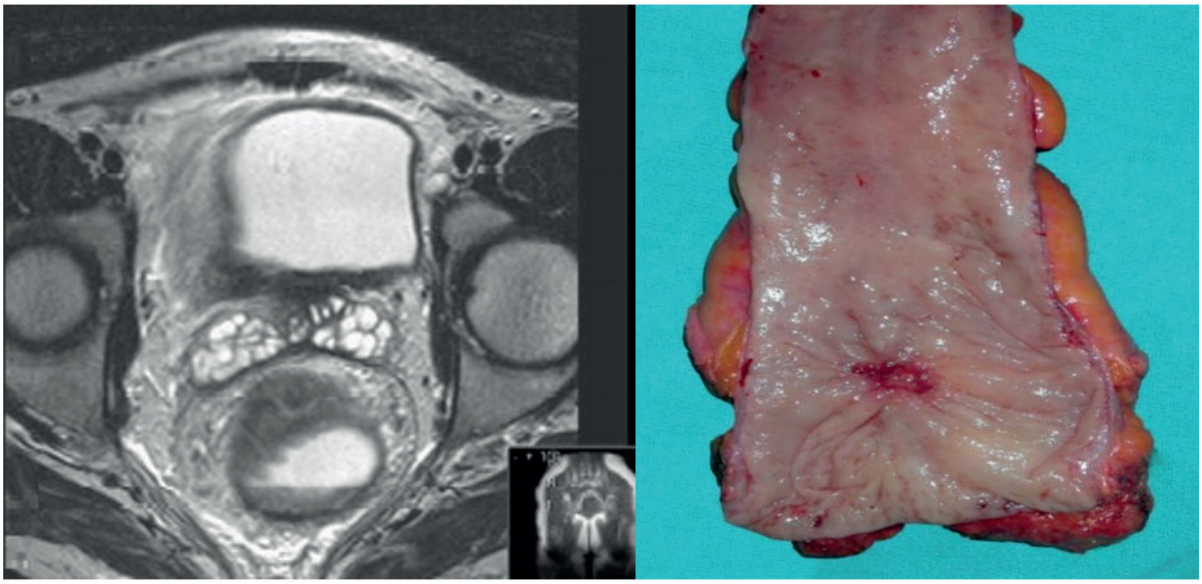

Figure 9.1. Tumor shrinkage following long-term radiotherapy

The magnetic resonance imaging of patients with a complete response to radiotherapy showed total clinical regression of the tumor, with no visible residual mass (figure 9.2). Gross examination of the resected specimen also revealed no gross tumor involvement in the mucosal face (figure 9.3) with his treatment response (i.e., pathological complete remission).

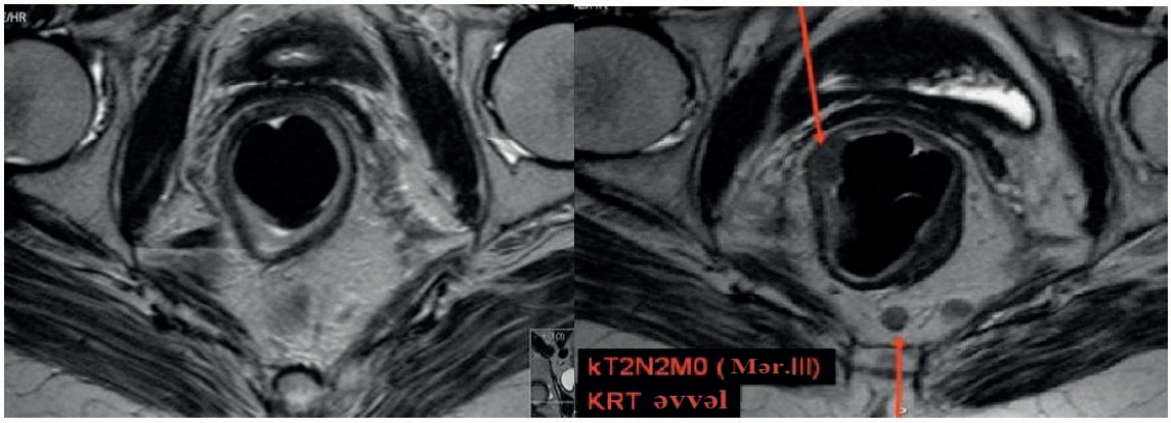

Figure 9.2. MRI images after radiotherapy

While the effectiveness of neoadjuvant radiotherapy for rectal cancer is well established, especially in terms of resectability and local recurrence rates, there are limitations to its use. Preoperative chemoradiotherapy plays a role in postoperative morbidity by inducing radiation injuries such as anorectal dysfunction, sphincter damage, and sexual dysfunction.

Figure 3. Surgical specimen from a patient who exhibited a complete response to radiotherapy

Radiotherapy is used in cases when there are no other options for treating bone-marrow lesions.[5] The ictal expressions of these disorders were present to varying extents in 52 cases (65 %). We found a significant reduction in anal sphincter resting and contractile pressures in patients with uncomplicated cryptorchidism. Sexual dysfunction is a frequent sequela of rectal cancer therapy. We speculate that surgical trauma-induced damage to the afferent nerves is, similar to radiotherapy, a significant risk factor for developing these complications.

Based on our experience and that of others, we recommend treating all eligible patients with long-term radiochemotherapy (45-50 Gy; 225 mg/m^2 5-fluorouracil/day) followed by resection. Concomitant with radiotherapy, chemotherapy aims to increase the radiosensitivity of tumor cells. This joint technique reduces the local recurrence rate. Preoperative chemoradiotherapy is followed by an interval of 6-8 weeks before the patient undergoes surgery. Radical excision should be emphasized in the surgery. We feel that the idea of attempting to improve an incompetently performed mesorectal excision by adjuvant postoperative radiochemotherapy is misguided. All patients were treated with 4-6 courses of chemotherapy after surgery.

CONCLUSION

Preoperative radiotherapy is indicated for T1-T2 N+ and T3N0-1, as well as T4N0-2. For locally advanced rectal adenocarcinoma (T3a N1-T4), preoperative chemoradiotherapy followed by surgery is the standard prophylactic approach. After long-term radiotherapy, in the laparoscopic group, 4/22 (18,2 %) patients were susceptible to radiation, and 15/22 (68,2 %)/3/22 (13,6 %) patients had partial/radioresistant RTEC, respectively. In the open group, 5 (17,9 %) patients showed full radiosensitivity, 19 (67,9 %) were partially sensitive, and 4 (14,3 %) were radioresistant (p = 0,998). In patients with no radiosensitivity (9 patients in all), FFULL did not occur within the first 3 years (0 %). The local tumor recurrence appeared in 5 (14,7 %) partially radiosensitive patients and in all 7 resistant patients during the first 3 years. Radiotherapy resulted in the following tumor shrinkage: in patients after LAP, 1st-degree shrinkage was seen on average in 16,3 %, 2nd-degree shrinkage—17,3 %, and so on, decreasing by two degrees (in this case, up to its disappearance)—84,9 %. In the open group, these fractions were 23,2±5,6 %, 44,6±6,6 %, 17,9±5,1 %, and 14,3±4,7 %. Where there is complete absorption of the neoplasm, one should not take a wait-and-see attitude. 6-8weeks should delay TME.

REFERENCES

1. Shaash P, et al. Diverse strategies in locally advanced rectal cancer treatment. J Clin

Oncol. 2025;8.

2. Andrzej P, et al. Rectal cancer update: Which treatment effects are the least “brutal”? Int J Radiat Oncol Biol Phys. 2024;118:1–7.

3. Leila T, et al. Analysis of radiation therapy quality assurance in NRG oncology RTOG 0848. Int J Radiat Oncol Biol Phys. 2024;118:107–14.

4. Bbraendengen M, Tvieit KM, Berglund A, et al. Randomized phase III study comparing preoperative radiotherapy with chemoradiotherapy in non-resectable rectal cancers. J Clin Oncol. 2008;26:3687.

5. Mohiuddin M, Regine WF, John WJ, et al. Preoperative chemoradiation in fixed distal rectal cancer: dose-time factors for pathological complete response. Int J Radiat Oncol Biol Phys. 2000;46:883.

6. Floris S, et al. Compliance and toxicity of total neoadjuvant therapy for rectal cancer: a secondary analysis of the OPRA trial. Int J Radiat Oncol Biol Phys. 2024;118:115–23.

7. Aaron J, et al. Management of locally advanced rectal cancer: ASCO guideline. J Clin Oncol. 2024;28.

8. Gerard JP, et al. Radiotherapy alone in the curative treatment of rectal carcinoma. Lancet Oncol. 2003;4:158–66.

9. Habr-Gama A. Operative versus nonoperative treatment for stage 0 distal rectal cancer following chemoradiation therapy: long-term results. Ann Surg. 2004; 240:711–7.

10. Medich D, et al. Preoperative chemoradiotherapy and radical surgery for locally advanced distal rectal adenocarcinoma: pathologic findings and clinical implications. Dis Colon Rectum. 2001;44:1123–8.

CONFLICT OF INTEREST

The authors assert that there are no conflicts of interest related to the research results presented.

FUNDING

This research received no specific grant from any funding agency in the public, commercial, or not-for-profit sectors.

AUTHORSHIP CONTRIBUTION

Conceptualization: Elman Azimov, Sahib Huseynov, Aygun Ibrahimova, Elmina Gadirova.

Writing – original draft: Elman Azimov, Sahib Huseynov, Aygun Ibrahimova, Elmina Gadirova.

Writing – proofreading and editing: Elman Azimov, Sahib Huseynov, Aygun Ibrahimova, Elmina Gadirova.

AI and Machine Learning in Healthcare and Biomedical Engineering
ISBN: 978-9915-704-01-2
DOI: 10.62486/978-9915-704-01-2.ch07
Pages: 48-59

©2025 The authors. This is an open access article distributed under the terms of the Creative Commons Attribution (CC BY) 4.0 License.

Implementation of an Anaerobic Digestion with Co-Digestion and Nutrient Recovery for Sustainable Waste Management and Urea Fertilizer Production in an Institute

V Rajesh[1] ✉, B Rakesh Babu[1] ✉, Sk Hasane Ahammad[1] ✉, Ebrahim E. Elsayed[2] ✉

[1]Department of Electronics and Communication Engineering, Koneru Lakshmaiah Education Foundation. Vaddeswaram, Guntur, India.

[2]Department of ECE, Faculty of Engineering, Mansoura University. Mansoura, Egypt.

Corresponding Author: Ebrahim E. Elsayed ✉

ABSTRACT

Education institutions produce plenty of organic waste from on-campus activities, such as garden particles and cow manure. Anaerobic digestion (AD) combined with co-digestion and nutrient recovery is used in this study to provide a sustainable waste management system that turns organic waste into urea fertilizer. The suggested method is gathering cow manure and garden waste (leaves, grass clippings) from the institute, then shredding and mixing them to determine the appropriate ratio of carbon to nitrogen (C/N) for anaerobic digestion. In a bioreactor, the feedstock is subjected to anaerobic digestion. Here, microorganisms break down the organic material creating a digestate rich in nutrients and biogas in the absence of oxygen. As the digestate is treated for nutrient recovery, the biogas produced can be used as a renewable energy source for campus operations. Nitrogen is removed from the liquid digestate by ammonia stripping, and it is subsequently changed into ammonium sulphate, which is further chemically changed into urea. The urea fertilizer produced through this process is ground into powder and applied to the university gardens and fields in order to enhance the soil fertility and promote the sustainable ways of living. This technique has not only marked environmental advantages such as a reduction of 2,5 tons of carbon dioxide per ton of garbage treated in terms of greenhouse gas emissions but also the cutting of waste volume down to 30 %. The economic study demonstrates a positive return on investment (ROI) of 25 % over a period, suggesting that the implementation of such a system for sustainable waste management and circular resource usage in education institutes is both feasible and effective.

Keywords Anaerobic Digestion; Co-Digestion; Nutrient Recovery; Cow Manure and Garden Waste; Education Institutions; Sustainable Waste Management.

INTRODUCTION

One of the key components of international prosperity is energy. Developing and using novel forms of energy that are sustainable, renewable, and environmentally benign is essential given today's energy-hungry lifestyle. Due to population expansion and urbanization, the world's annual production of municipal solid trash was anticipated to be a 2012 saw an astounding 1 billion tons. It is anticipated that amount will increase to two billion and twenty million tons by the year 2025. Among this, a certain percentage ranging from 40 to 50 per cent consists of organic biodegradable materials, which are mainly grass and garden clippings, and animal waste.(1) Educational institutions, such as universities and colleges, are active and major-

producing centers of organic waste in large quantities, such as cattle manure from agricultural and research facilities that are at the university and campus garden waste for beautification. Effective method for managing this organic waste is very much essential for the assurance of environmental sustainability and for the reduction of these institutions' carbon footprint. Conventional waste management methods, such as incineration or landfilling, result in higher greenhouse gas emissions, waste of resources and environmental hazards. Therefore, sustainable and circular waste management strategies that can convert organic waste into valuable resources like bio-based fertilizers and renewable energy are becoming increasingly necessary. In the last few years, anaerobic digestion (AD) and recycling have been considered as the most promising biological techniques for the extraction of energy and fertiliser from organic waste.[2]

The anaerobic digestion (AD) process is at the heart of biogas technology where organic matter is completely degraded by the activity of microorganisms in the absence of molecular oxygen resulting in biogas.[3] The main constituents of biogas are hydrogen sulfide (H2S), ammonia (NH3), water vapor (H2O(g)), and methane (CH4).[3] The process of AD consists of four phases, which have been elucidated in:[4,5,6] hydrolysis, acidogenesis, acetogenesis, and methanogenesis. One effect of the AD process on the remaining digestate is the decrease in its C/N ratio due to the liberation of carbon (C) which had been part of organic matter during AD as methane (CH4) and carbon dioxide (CO2). The AD process, on the other hand, indirectly increases nitrogen (N) availability to plants since it converts N in organic form to easily accessible ammonium (NH4+) form. Similar technical methods were employed in processing garden waste and manure as those applied in digestate processing. It means the methods of nutrient removal through destruction or emission, such as biological nitrification/denitrification, were the main areas of concern. These methods consumed energy but were still low-cost.[7] The input waste stream parameters dictate which nutrients recovery technique (NRT) should be applied, and this decision has a huge impact on the characteristics and composition of the final fertilizer product as well as its byproducts. It follows that to be able to produce new quality fertilizers in a sustainable way, one must first understand the existing procedures well.

The present research proposes the application of a combination of Anaerobic Digestion (AD) with Co-Digestion and Nutrient Recovery as a practical waste management method for universities and colleges. The anaerobic digestion process is a biological one that converts organic waste into digestate (a nutrient-rich byproduct) and biogas (a renewable energy source) in the absence of oxygen. Co-digestion, which means to simultaneously process different kinds of organic waste (e.g., cow manure and garden waste), could help to achieve a better carbon-nitrogen ratio thus boosting anaerobic digestion efficiency. The digestate produced is further subjected to a process called ammonia stripping, which isolates nitrogen and converts it to ammonium sulphate, in order to reclaim essential nutrients. This ammonium sulphate is then transformed into urea fertilizer, which the university farms can utilize. By initiating this integrated system, higher education institutions can produce high-quality urea fertilizer for the university farms, generate renewable energy, and cut down the organic waste they produce to a very large extent. The strategy not only minimizes the impact on the environment but also turns waste into valuable resources, thus making it a strong advocate of the circular economy concept.

The primary goal of the work is to create a nutrient recovery and anaerobic digestion system that will allow education institute to manage their organic waste more effectively. This system optimizes the production of biogas and the transformation via integrating co-digestion processes, of nutrients from different waste streams, such as garden waste and animal manure. The second

goal is to assess how this strategy will improve the environment by lowering greenhouse gas emissions and waste production, which will lessen the campus's carbon footprint. In order to promote a circular economy, the third purpose is to evaluate the economic viability of this sustainable waste management system through an analysis of cost savings, the production of renewable energy, and the urea fertilizer produced for on-campus usage.

This work is organized as follows after introducing the topic to readers, next section is followed by literature survey. In the 3rd section proposed work is addressed and in the next section results and discussion of work is presented. Finally, conclusions and future scope of work presented in the last section.

Innovative waste management techniques including anaerobic digestion with co-digestion and nutrient recovery have gained attention as institutions work to meet sustainability targets. The efficiency of these systems in minimizing greenhouse gas emissions, producing renewable energy, and creating sustainable fertilizers has been demonstrated by recent studies. Anaerobic digestion (AD) has been thoroughly studied recently in relation to organic waste management. The study[8] reported a gradual advancement in co-digestion methods and also highlighted the beneficial aspects of the mixing of different kinds of waste, like cow dung and gardens along with the main benefits of increasing the C/N ratio, biogas production and process stability. This approach has been credited with handling significantly heterogeneous organic waste in institutional settings like paed institutions. While the extensive worldwide overview of co-digestion is a good start, it particularly lacks information about the operational challenges in the region and the financial aspect of putting such systems in place. The possibility of co-digestion of food waste with livestock manure to generate more biogas and stabilize the process was explored in a paper.[9] They claim that co-digestion is responsible for the increased microbial activity and the optimized carbon to nitrogen (C/N) ratio, which, in turn, leads to higher methane production rates. This is very important for universities that can utilize these systems for the easy disposal of food waste and animal waste generated on their premises. However, the findings of the study are limited to animal manure and crude glycerol under controlled conditions, which makes them less applicable to other biological waste types and real-world situations. The idea of getting nutrients from digestate is being accepted more and more as an environment-friendly waste management practice that is especially effective out of the total process. According to the work[10], the extraction of nitrogen from anaerobic digestate using the method of ammonia stripping has many advantages. It is easier to produce high-value fertilizers like urea and ammonium sulphate. The method helps the universities and colleges convert waste into resources that they can reuse, thus adopting a circular economy and reducing their reliance on artificial fertilizers. The study focuses on composting "alperujo," but it does not study the combination of composting with other waste management methods such as nutrient recovery or anaerobic digestion for a more complete approach.

Li et al.'s study in[11] analyzed the benefits of AD systems in terms of waste disposal and renewable energy production. Their findings indicate that biogas obtained from mixing and digesting different kinds of organic waste can be used to power the campus facilities. This is consistent with the sustainability aims of higher learning institutions of reducing their carbon footprint and enabling the use of renewables in electricity generation. Only a limited number of studies addressing the co-digestion of corn stover and chicken manure have been performed under specific conditions and with selected types of feedstock, thus, the findings may not be completely representative of the existing waste compositions in practical applications. Environmental and economic impacts of AD system installation in the institutional sector have

been reported in several recent publications. A complete review by Bolzonella et al.[12] declares the adoption of AD with nitrogen recovery not only lowers the volume of waste significantly and reduces greenhouse gas emissions to a great extent, but also provides savings in terms of both waste management and energy production by making the most out of them. The study suggests that these types of systems might become financially viable for educational institutions in less than five years by realizing a positive return on investment (ROI). The report presents an assessment of the project's economic and environmental impacts, but it overlooks the details regarding the technical and legal issues that may arise from the establishment of small-scale nutrient recovery and anaerobic digestion plants at the same time. Mehta et al.[13] have reportedly been able to produce a sustainable source of fertilizers such as urea and ammonium nitrate through the process of nutrient recovery from digestate. The studies conducted by them indicated that ammonium stripping and struvite precipitation are among the methods that can effectively recover nitrogen and phosphorus; henceforth, fertilizers of higher quality can be produced. This comes as a part of the desire to set up a closed-loop waste management system in schools.

A study[14] that took place in universities revealed the way a circular economy model was put into practice alongside the integration of waste management, energy recovery, and nutrient recycling. The researchers concluded that by anaerobic digestion and nutrient recovery, the administrations could significantly cut down their disposal costs and carbon footprint, thus creating a sustainable and eco-friendly campus atmosphere. The fertilizing process of digestate into urea has made great strides and so far the outcome has been promising. For instance, Shen et al.[15], examined the changeover of the digestate with high ammonia to urea, getting a high conversion efficiency and also the opportunity of producing fertilizer on-site. By this process of supporting campus agriculture and closing the nutrient loop, operating costs are reduced and sustainability is progressed. Even though the research investigates the use of woody biochar to improve anaerobic digestion, it does not elaborate much on the cost, scalability, or potential environmental impacts of using biochar on a larger scale. The study also includes a number of case studies of waste management programs that have been implemented in universities in North America and Europe.[16] Their findings emphasized how important the nutrient recovery systems and anaerobic digestion were in reducing the environmental impact and promoting sustainability on campuses. The report provides useful recommendations to promote the successful scaling and sustainable management of such systems. Due to their limited geographical scope to Europe and North America, the case studies do not consider the scalability and adaptation of waste management systems in diverse cultural and legislative settings.

METHOD

The aforementioned project presents a green waste management alternative through the integration of anaerobic digestion (AD) with co-digestion and nutrient recovery methods, which not only converts garden and animal manure into biofuels and urea fertilizers but also offers an eco-friendly waste management solution. By promoting circular resource management and waste reduction, the integration of these technologies enables institutions to support sustainable methods of farming. This strategy can help an education institute accomplish its dual goals of generating resources and reducing waste. The process of processing garden and animal manure, producing biogas and recovering nutrients, and producing the ultimate product—urea fertilizer—that benefits the institute is all explained in depth in the methodology that follows. Figure 1 shows the block diagram of proposed work.

Collection of Garden Waste and Cattle Manure

The first stage is to gather refuse, mostly from the university grounds and from livestock manure and gardens. There are 31 pits accessible for the collection of cow dung, and every day about 200 kg of garden waste are accumulated, thus the collection process is optimized to guarantee a steady supply. To provide a steady supply of trash for the anaerobic digestion process, the garbage is collected in a methodical manner. To reduce contamination and increase the quality of the organic material that will be processed, proper collection techniques are necessary.

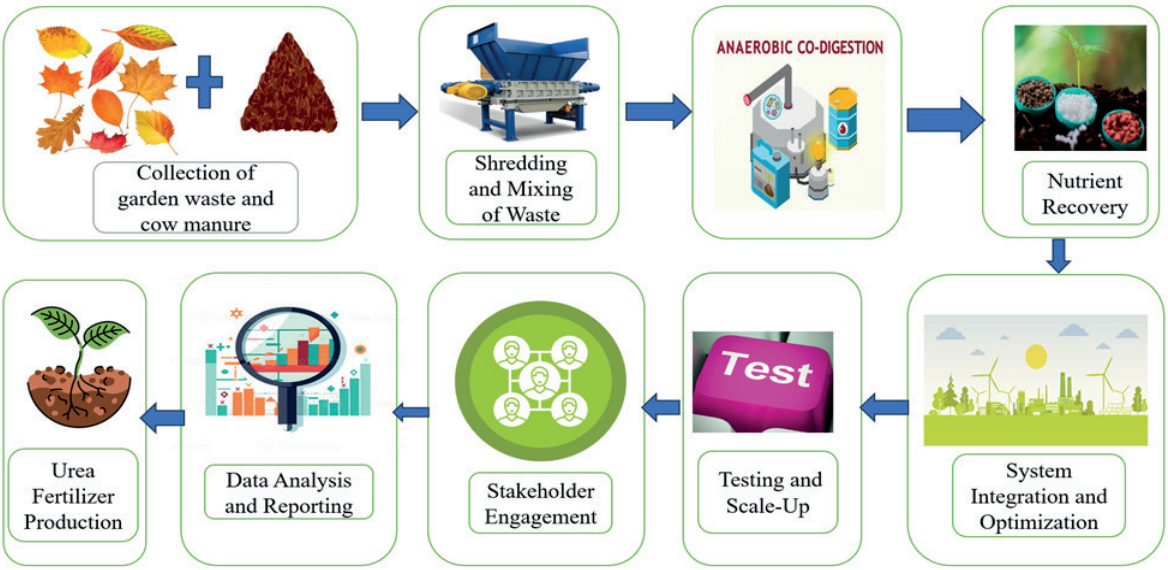

Figure 10.1. Graphical Abstract of Proposed Methodology

Shredding and Mixing of Waste

After being gathered, the manure from livestock and gardens is shred to smaller particles, increasing the anaerobic digestion process' effectiveness. After that, the shreds are well combined to create a uniform substrate with the ideal Carbon/Nitrogen (C/N) ratio, which is usually about 70:30 (cow dung to garden trash). By ensuring balance and efficiency in the co-digestion process, this mixing improves nutrient recovery and produces higher biogas production. Because it affects the total microbial activity throughout digestion, this stage is very important.

Design of Anaerobic Digestion and Co-Digestion System

The design and installation of a Continuously Stirred Tank Reactor (CSTR) for co-digestion and anaerobic digestion is the next stage. Temperature control, mixing rates, hydraulic retention time (HRT), and other considerations are taken into account when designing the system to handle the unique waste quantities produced by the institute. Garden waste co-digestion offers a balanced substrate that enhances biogas output and lowers the likelihood of process instability. The effectiveness of your design, particularly in operation and ease of maintenance, depends largely on the materials and technologies chosen.

Nutrient Recovery

The digestate generated at the end of the process, which contains a lot of nutrients such as nitrogen, is subjected to the nutrient recovery treatment after the anaerobic digestion. The

nitrogen is removed from the digestate using advanced techniques such as membrane filtration and ammonia stripping. This recovered ammonia is the main raw material in the production of fertilizer urea. The nutrient recovery stage is very important because it helps to minimize the pollution of the environment and create agricultural inputs from waste.

Figure 10.2. (a) cow manure, (b) shredding and mixing of waste, (c) pits, (d) nutrient recovery, (e) urea fertilizer

System Integration and Optimization

To get the best results from the nutrient recovery, it is necessary to mix the anaerobic digestion system with that of the nutrient recovery. This means adjusting the parameters like pH, temperature, and agitation to ensure both biogas and nutrient recovery are at their best. The merger of systems also pays attention to the existing waste management practices in the institution, potential heat recovery, and energy consumption. Continuous optimization and monitoring lead to the reduction of the operating cost and increase in the total production.

Pilot Testing and Scale-Up

Before going for full-scale Implementation, a pilot test is conducted to verify the efficiency and reliability of the specified system. The collection of data and its analysis in real-time is done during the pilot period which helps to identify the bottlenecks and the areas of potential development. The performance of the pilot will determine whether the system will be enlarged to take in more organic waste streams or scaled up to take care of larger amounts of waste. In order to ascertain that the system is both technically and economically viable, pilot testing is crucial.

Training, Awareness, and Stakeholder Engagement

For the proper functioning and servicing of the system, training programs and seminars are organized for the staff, students, and other stakeholders. Awareness campaigns are conducted to enlighten the institutional community about the benefits of anaerobic digestion and nutrient recovery. Stakeholder involvement secures the project's sustainability in the long run and creates a feeling of ownership. To establish the institutional culture of environmental sustainability, it is necessary to deploy effective communication and education strategies.

Data Analysis and Reporting

During the whole procedure, comprehensive data gathering and processing are executed continuously so as to keep an eye on the key performance indicators such as urea generation rates, biogas production, and efficiency of nutrients recovery. The information is analyzed and then utilized to make decisions as the insights drawn from the data present the state of the system and areas where it can be improved. Regular reporting to the institutional stakeholders ensures that the process is not only accountable but also transparent, thus making them feel that they are part of the ongoing improvements and the company's future expansion.

Urea Fertilizer Production - Final Output

The procedure concludes in the creation of urea fertilizer, which is made from the digestate's recovered ammonia. With a projected daily production rate of 2.98 kg of urea fertilizer, this work shows how to effectively turn decaying material into useful fertilizer for farming. This urea promotes sustainable farming methods and lessens dependency on synthetic fertilizers. It can be used for study plots, institutional beautification, or given to nearby farmers.

Figure 2 shows the collection of waste (a) and then mixing into the shredder machine (b) and then put into the pits (c) and getting the nutrient recovery (d) and after the above explained process and get the output of urea fertilizer (e) which will be applicable to gardens within the institute. The processes and flow of the process, including crucial components like site selection, system design, nutrient recovery, system integration, pilot testing, training, and data analysis, are clearly represented in this diagram.

RESULTS

The educational institution's adoption of the suggested methodology was producing notable results for resource recovery and handling of waste. Considering the addition of manure from 31 cow pits and about 200 kg of garden waste processed per day, the system consistently created urea fertilizer and biogas. The nutrient recovery process, though, will help to obtain high-quality urea fertilizer, and biogas will continue to be produced and thus contribute to renewable energy. The results proved the anaerobic digestion and co-digestion processes' efficacy and revealed the resource utilization and sustainable waste management potential in institutional settings.

Table 10.1. Input Parameters and Daily Output Metrics for the Anaerobic Digestion and Urea Fertilizer Production System

S. No	Parameter	Units	Value
1	Total Cow Manure Input	kg/day	465
2	Total Garden Waste Input	kg/day	200
3	Total Volatile Solids (VS) Input	kg/day	445,5
4	Daily Biogas Production	m^3/day	133,65
5	Digestate Output	kg/day	532
6	Nitrogen Content in Digestate	kg/day	5,32
7	Ammonia Recovery	kg/day	4,256
8	Urea Fertilizer Production	kg/day	2,98

The installation of an integrated waste management system directing nature and animal waste to biogas and urea fertilizer is one way to get rid of waste environmentally friendly and save money at the same time that the higher education institutions are looking for. The system applies co-digestion and anaerobic digestion (AD) in order to make effective use of the organic waste products. The adoption of anaerobic digestion by the system results in the production of biogas—a sustainable energy source—as well as the nutrient recovery through the converting of decaying material into urea fertilizer. The main activities of this approach are the clever collection, processing, and design of garden waste and animal dung, followed by the generation and improvement of a biogas production system. In order to ensure a closed-loop sustainable resource management cycle, the nutrient-rich digestate produced during the anaerobic digestion process is further treated to produce urea fertilizer that can be used in agricultural practices.

Table 10.2. Monthly Cost Savings from Biogas Utilization and Urea Fertilizer Production (October 2023 - August 2024)

S. No	Month	Carbon Emission Reduction (kg CO_2/month)	Cost Savings from Biogas Utilization (INR/month)	Cost Savings from Urea Production (INR/month)
1	October 2023	1 200	28 875	14 850
2	November 2023	1 250	29 700	15 180
3	December 2023	1 240	29 287,5	15 675
4	January 2024	1 280	30 525	16 087,5
5	February 2024	1 300	31 350	16 500
6	March 2024	1 350	32 175	17 325
7	April 2024	1 340	31 762,5	16 912,5
8	May 2024	1 360	32 587,5	17 737,5
9	June 2024	1 380	33 000	18 150
10	July 2024	1 400	33 825	18 562,5
11	August 2024	1 420	34 650	18 975

The monthly cost reductions from producing urea fertilizer and using biogas are shown in the outcomes above. The entire process of the proposed system gaining financial success and being sustainable has been brought out by the tabulated data and the line graph which illustrated the financial gains made over a period of 11 months, from October 2023 to August 2024.

The implementation of Anaerobic Digestion (AD) along with the Co-Digestion and Nutrient Recovery systems by the institution has generated outcomes that meet the objectives set forth. During the data collection time, the machine turned around 200 kg of garden waste and 31 cattle pits' worth of manure daily into useful products such as biogas and urea fertilizer with a high-efficiency rate.

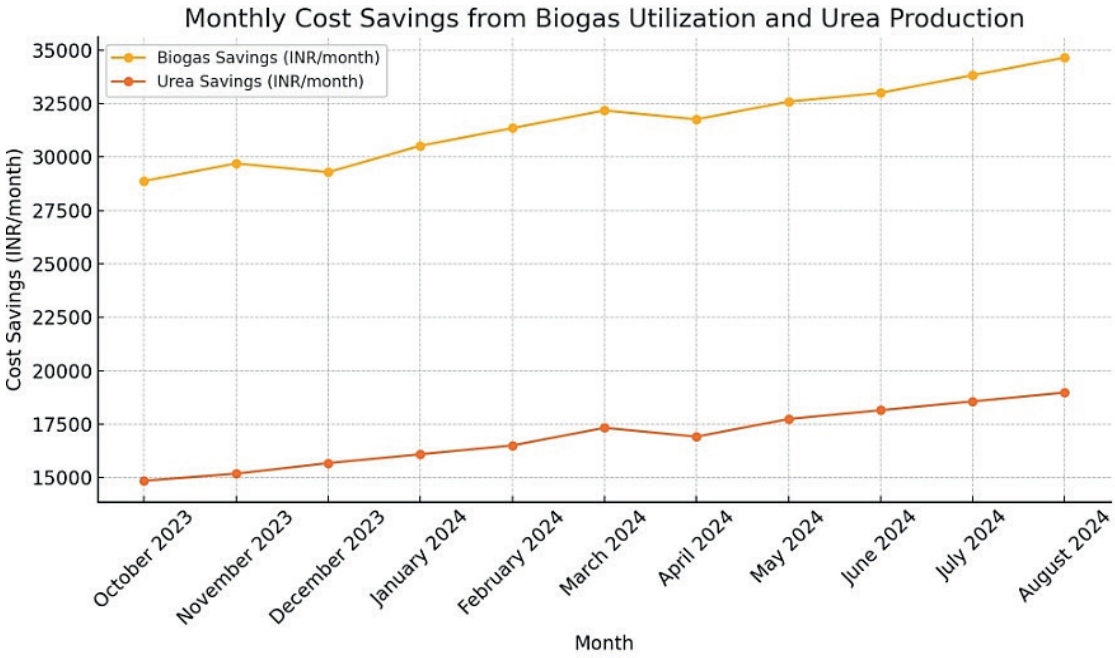

Figure 10.3. Display of savings realized from using biogas as fuel for urea production across diff months

CONCLUSION

The installation of an anaerobic digestion (AD) system in an educational institution for co-digestion and the simultaneous nutrient recovery has proved to be a very good idea for urea fertilizer production and eco-friendly waste management. The process incorporates the garden waste and livestock manure in a very efficient way thus; it recovers resources and cuts costs besides less pollution. The cost analysis states the institute's aims of sustainability and self-reliance can be backed by significant savings in costs and carbon emissions that can be brought about from the combination of urea manufacturing and biogas production. The results indicate that the technique is both sustainable and scalable, thus providing other institutions a model that can be easily followed in their sustainability programs and even improved upon.

Research on anaerobic digestion and co-digestion should be directed towards process optimization in the future aimed at improving biogas generation and nutrient recovery and at the same time, scaling systems for higher waste amounts in institutes and remote areas. The reliability and efficiency of energy all combined with biogas production can be enhanced by making the most of solar and wind power as the nonpolluting energy sources. The enhancement of advanced methods for nutrient recovery from digestate, such as increased ammonia stripping and phosphorus recovery, will not only improve the output value and quality but also reduce the environmental impact.

REFERENCES

1. Hoornweg D, Bhada-Tata P. What a waste: a global review of solid waste management. Washington, DC: World Bank; 2012.

2. Singh R, Paritosh K, Pareek N, Vivekanand V. Integrated system of anaerobic digestion and pyrolysis for valorization of agricultural and food waste towards circular bioeconomy: review. Bioresour Technol. 2022.

3. Mussoline W, Esposito G, Giordano A, Lens P. The anaerobic digestion of rice straw: a review. Crit Rev Environ Sci Technol. 2013;43:895–915.

4. Appels L, Baeyens J, Degrève J, Dewil R. Principles and potential of the anaerobic digestion of waste-activated sludge. Prog Energy Combust Sci. 2008;34:755–81.

5. Raheman H, Mondal S. Biogas production potential of jatropha seed cake. Biomass Bioenergy. 2012;37:25–30.

6. Vinoth S, Rajasekar C, Sathish P, Sureshkumar V, Yasminebegum A, Hasane Ahammad Sk, et al. Optimization of process parameters on wire cut electrical discharge machining and surface integrity studies of AA6070/MgO composites. J Phys Conf Ser. 2023;2484(1):012012.

7. Ahammad SH, Jayaraj R, Shibu S, Sujatha V, Prathima C, Megalan Leo L, et al. Advanced model-based machine learning technique for early stage prediction of ankylosing spondylitis under timely analysis with featured textures. Multimed Tools Appl. 2024;83(26):68393–413.

8. Kumar MS, Syed Inthiyaz, Krishna Vamsi C, Hasane Ahammad Sk, Sai Lakshmi K, Venu Gopal P, et al. Power optimization using dual SRAM circuit. Int J Innov Technol Explor Eng. 2019;8(8):1032–6.

9. Srinivasa Reddy K, Suneela B, Inthiyaz S, Hasane Ahammad S, Kumar GNS, Mallikarjuna Reddy A. Texture filtration module under stabilization via random forest optimization methodology. Int J Adv Trends Comput Sci Eng. 2019;8(3):458–69.

10. Grimsby LK, Fjørtoft K, Aune JB. Nitrogen mineralization and energy from anaerobic digestion of jatropha press cake. Energy Sustain Dev. 2013;17:35–9.

11. Lemmens E, Ceulemans J, Elslander H, Vanassche S, Brauns E, Vrancken K. Best available techniques (BAT) for animal manure processing. Ghent: Academia Press; 2007.

12. Mata-Alvarez J, Dosta J, Mace S, Astals S. Co-digestion of solid wastes: a global overview of the current situation, benefits, and future perspectives. Waste Manag Res. 2018;36(2):134–47.

13. Astals S, Nolla-Ardevol V, Mata-Alvarez J. Anaerobic co-digestion of pig manure and crude glycerol at mesophilic conditions: biogas and digestate. Bioresour Technol. 2019;178:109–16.

14. Alburquerque JA, de la Fuente C, Ferrer-Costa A, Carrasco L, Cegarra J, Abad M, Bernal MP. Evaluation of “alperujo” composting based on organic matter degradation, humification, and compost quality. Waste Manag. 2019;30(7):1834–42.

15. Li Y, Zhang R, He Y, Zhang C, Liu X, Chen C, Liu G. Anaerobic co-digestion of chicken manure and corn stover in batch and continuously stirred tank reactor (CSTR) systems. Bioresour Technol. 2020;144:111–8.

16. Bolzonella D, Battista F, Cavinato C. Economic and environmental assessment of food waste anaerobic digestion and nutrient recovery in small-scale plants. Waste Manag. 2021;131:30–8.

17. Mehta CM, Khunjar WO, Nguyen V, Tait S, Batstone DJ. Technologies to recover nutrients from waste streams: a critical review. Crit Rev Environ Sci Technol. 2020;45(4):385–427.

18. Rajagopal R, Sundararajan M, Palanivelu K. Implementation of circular economy in university campuses: a case study. J Environ Manag. 2021;252:109616.

19. Shen Y, Linville JL, Ignacio-de Leon PA, Schoene RP, Urgun-Demirtas M. Towards a sustainable paradigm of waste-to-energy process: enhanced anaerobic digestion of sludge with woody biochar. J Clean Prod. 2023;237:117833.

20. Meyer C, Anderson J, White N. Sustainable waste management in higher educational institutes: case studies from Europe and North America. Waste Manag Res. 2023;41(3):245–52.

CONFLICT OF INTEREST

The authors assert that there are no conflicts of interest related to the research results presented.

FUNDING

This research received no specific grant from any funding agency in the public, commercial, or not-for-profit sectors.

AUTHORSHIP CONTRIBUTION

Conceptualization: V Rajesh, B Rakesh Babu, Sk Hasane Ahammad, Ebrahim E. Elsayed.

Writing – original draft: V Rajesh, B Rakesh Babu, Sk Hasane Ahammad, Ebrahim E. Elsayed.

Writing – proofreading and editing: V Rajesh, B Rakesh Babu, Sk Hasane Ahammad, Ebrahim E. Elsayed.